processes

MDPI

Article

Influence of Foaming Agents and Stabilizers on Porosity in 3D Printed Foamed Concrete

Magdalena Rudziewicz, Marcin Maroszek, Adam Hutyra, Michał Góra, Karina Rusin-Żurek and Marek Hebda *

Faculty of Materials Engineering and Physics, Cracow University of Technology, Warszawska 24, 31-155 Kraków, Poland; magdalena.rudziewicz@doktorant.pk.edu.pl (M.R.); marcin.maroszek@doktorant.pk.edu.pl (M.M.); adam.hutyra@doktorant.pk.edu.pl (A.H.); michal.gora@doktorant.pk.edu.pl (M.G.); karina.rusin-zurek@pk.edu.pl (K.R.-Ż.)
* Correspondence: marek.hebda@pk.edu.pl

Abstract: This study examines the pore structure and distribution in 3D printed and cast foamed concrete using protein-based and synthetic foaming agents alongside various stabilizing additives. In 3D printed samples, pores are irregular and flattened due to mechanical forces during printing, whereas cast samples display uniform, spherical pores from homogeneous foam distribution. Samples containing the CA stabilizer show higher apparent densities (up to 2.05 g/cm^3 for printed samples), correlating with lower water absorption. Protein-based foaming agents (PS) produce smaller, more evenly distributed pores, while synthetic agents (AS) result in larger, less uniform pores. Stabilizers significantly influence pore characteristics: commercial stabilizers yield smaller, more uniform pores, while recycled industrial oil (UO) leads to larger, more variable pores. Protein-based agents improve structural stability and reduce water absorption through uniform pore distributions, while synthetic agents lower density and increase water absorption. The highest sorption values were observed in samples with AS without stabilizer (1.7 kg/m^{2}h^1 /^{2}) and AS and UO (1.6 kg/m^{2}h^1 /^{2}) in a vertical orientation, with the horizontal orientation of sample AS and UO achieving a peak value of 2.0 kg/m^{2}h^1 /^{2}. Moreover, stabilization using UO resulted in higher sorption coefficients than stabilization with CA. High porosity in M1 resulted in low strength (0.2 MPa bending, 0.1 MPa perpendicular compression), while M5 showed superior performance (11.5 MPa perpendicular compression). PS-foamed samples (M4, M6) with uniform pores had the highest strengths, with M6 achieving 3.8 MPa bending and 10.3 MPa perpendicular compression. Perpendicular compression (M5: 11.5 MPa) was up to three times stronger than parallel compression due to weak interlayer bonds in 3D printing.

Keywords: foamed concrete (FC); foam stability; foam lifetime; lightweight concrete; foaming agents; foam stabilization

check for updates

Academic Editors: Frank Alifui-Segbaya and Suhas Alkunte

Received: 9 January 2025
Revised: 28 January 2025
Accepted: 30 January 2025
Published: 3 February 2025

Citation: Rudziewicz, M.; Maroszek, M.; Hutyra, A.; Góra, M.; Rusin-Żurek, K.; Hebda, M. Influence of Foaming Agents and Stabilizers on Porosity in 3D Printed Foamed Concrete. *Processes* **2025**, *13*, 403. https://doi.org/10.3390/pr13020403

Copyright: © 2025 by the authors. Licensee MDPI, Basel, Switzerland. This article is an open access article distributed under the terms and conditions of the Creative Commons Attribution (CC BY) license (https://creativecommons.org/licenses/by/4.0/).

1. Introduction

In recent years, foamed concrete has garnered significant attention due to its ability to merge the benefits of traditional construction materials with the lightweight and insulating properties inherent to porous structures. The porous nature of foamed concrete imparts superior thermal and acoustic insulation, along with reduced structural loads, compared to conventional materials. However, achieving optimal performance requires a meticulous regulation of porosity, including the control of pore size, distribution, mechanical strength, and thermal conductivity—parameters directly influenced by the size and interconnectivity

of pores within the material [1–4]. Research has demonstrated that increasing porosity and average pore size generally leads to reductions in mechanical strength and thermal conductivity, emphasizing the critical trade-offs involved in material design. For practical applications, such trade-offs play a crucial role in determining the suitability of foamed concrete for specific uses. For example, in 3D printed structural components, where customized geometries and rapid prototyping are key advantages, controlling porosity is critical for balancing weight reduction with adequate load-bearing capacity. In applications such as wall panels, tunnel cover panels, or partition blocks, high porosity can enhance thermal and acoustic insulation, making the material ideal for energy-efficient buildings. Conversely, components subjected to higher structural loads, such as load-bearing walls or support columns, require a lower porosity to ensure mechanical integrity. The findings highlight the need for tailored formulations in foamed concrete to meet application-specific requirements. Advanced manufacturing techniques, such as 3D printing, enable precise control over the distribution and size of pores, facilitating the optimization of both mechanical and thermal performance. By understanding these trade-offs, engineers and architects can better integrate foamed concrete into diverse construction scenarios, achieving a balance between functionality, sustainability, and cost-efficiency.

The production process of foamed concrete introduces several challenges, particularly in maintaining foam stability during manufacturing. Foam volume and stability are critical for ensuring homogeneity, consistent pore structures, and desired material properties. Excessive foam content often leads to coalescence during mixing, producing larger, irregular pores and diminishing mechanical integrity. Foam instability can arise due to variations in mixture viscosity, interactions between components, or the effects of chemical activators. Mechanisms of foam degradation—such as drainage, coalescence, and bubble overgrowth—are well documented and have significant implications for the material's structural properties [5–7]. These processes must be controlled to achieve a balance between porosity and strength. Drainage occurs when the liquid within the network of interfaces is driven by gravity, leading to the separation of gas and liquid phases. This process reduces foam density and separates the liquid phase, ultimately resulting in a dry state characterized by polyhedral bubbles. The reduction in drainage is enhanced by increased liquid viscosity, which can be achieved by incorporating a viscous solution into the liquid phase. Such modifications increase the internal pressure within the bubbles, thereby reducing their size. Notably, smaller bubble radii correspond to higher internal pressures. Drainage and diffusion represent the primary mechanisms of foam degradation, alongside coalescence. Coalescence is a physical phenomenon wherein liquid droplets, gas bubbles, or solid particles merge to form a single, larger entity. Adjacent bubbles coalesce when the interstitial film ruptures due to aging processes [8–11]. Another significant degradation mechanism is bubble overgrowth, in which gas migrates from smaller higher-pressure bubbles to larger lower-pressure bubbles. Over time, this leads to the expansion of larger bubbles and the dissolution of smaller ones. This phenomenon can have detrimental effects, including reduced concrete strength, compromised insulation properties, and difficulties during material extrusion. These limitations hinder the commercialization and widespread application of foamed materials. Therefore, the development of effective foam stabilization techniques is essential to prevent air bubble growth and to maintain fine pores in both fresh and hardened mixtures. To address the challenges of foam instability, surfactants are frequently employed as stabilizing agents. These compounds reduce surface tension, thereby improving the wetting and flow characteristics of concrete mixtures. Surfactants are categorized by their ionic character (anionic, cationic, nonionic, or amphoteric) and origin (natural or synthetic) and serve as emulsifiers, dispersants, and foaming agents [12]. Numerous studies have explored the use of micro- and nano-sized solid particles in foamed

concrete, including nano-silica [13,14], nano-calcium carbonate [13], nano-alumina [15], nano-Al_2O_3 [16], starch [17], and carbon quantum dots (RHBCDs) [18]. Additionally, used engine oil (UEO) has been employed to enhance foam stability [19]. Recent research highlights that the combined use of surfactants, Janus-ZrO_2 nanoparticles, and hydrophilic SiO_2 facilitates the synthesis of ultra-stable foams [20]. While nanoparticle-modified foams exhibit reduced flowability and increased viscosity in foamed concrete, their incorporation can lead to higher foam density and cost increases. These nanoparticles can also modify the Ca/Si ratio in pore walls and influence cement hydration, thereby enhancing the strength of foamed concrete [4]. The effects of various anionic surfactant-based foaming agents on foam properties have been extensively studied, including ammonium lauryl sulfate (ALS) [21], triethanolamine laurylsulfate (TLS) [21], sodium lauryl sulfate (SLS) [22], sodium dodecyl sulfate (SDS) [23], alpha olefin sulfonate (AOS), sodium lauryl ether sulfate (SLES), and sodium alcohol ether sulfate (AES) [24]. Nonionic surfactants, such as Tween 80 (polyoxyethylene (20) sorbitan monooleate—$C_{64}H_{124}O_{26}$) and Triton X-100 (polyethylene glycol tert-octylphenyl ether—$C_{14}H_{22O}(C_2H_4O)$n, n = 9–10) have also been utilized to stabilize fresh geopolymer foam [25]. Moreover, stabilizing agents like xanthan gum [26], carboxymethyl cellulose (CMC) [27], and hydroxypropyl methylcellulose (HPMC) have been shown to improve foam stability by reinforcing the liquid film. HPMC, a commonly used thickening agent in concrete and mortars, enhances both foam stability and flow characteristics [28–30]. Investigations into the impact of HPMC on the rheological properties and constructability of 3D printed foamed concrete (3DPFC) reveal that HPMC improves yield stress and constructability by promoting the agglomeration of cement particles into larger flocs [31]. The influence of various factors, including the water–cement ratio and foam volume [32–34], size of aggregates [35], the addition of fibers [36], pore size [37], the partial replacement of cement with fly ash, and other additives [38], on the strength properties of foamed concrete has been investigated. For mixtures intended for 3D printing, aggregates larger than 4 mm must be excluded, as they can negatively impact shrinkage during the drying process of successively printed layers. Shrinkage is further influenced by the cement-to-filler ratio, the type of filler used [39], foam volume, and the choice of foaming agents [40]. On the other hand, there is a lack of comprehensive studies of drying shrinkage in foamed concrete incorporating recycled materials for additive manufacturing, particularly concerning the use of various foaming agents. Moreover, while significant research has been conducted on the development of stable foamed concrete, the large-scale testing of foamed concrete materials containing construction waste for 3D printing applications remains limited. The effective incorporation of recycled products into stable foamed materials holds great potential to revolutionize structural design and construction, offering more sustainable alternatives for building materials and methods. Therefore, further investigation into foam stabilization techniques is crucial for improving the properties and performance of these materials, especially in the context of their use in additive manufacturing technologies [41]. Air voids introduced into fresh concrete mixtures for the preparation of controlled products, such as foamed concrete, cellular concrete, or autoclaved aerated concrete, can create capillary, gel, or randomly trapped pores. Foamed concrete is typically produced using either mechanical or chemical methods. Chemical aeration involves the addition of gas-releasing substances, such as aluminum (Al) or zinc (Zn) powders, hydrogen peroxide (H_2O_2), or silicon (Si), to the cement paste. These substances generate gasses like hydrogen (H_2) or oxygen (O_2), which create air voids within the concrete. In contrast, mechanical aeration is achieved by either introducing pre-prepared foam into the cement paste or by vigorously mixing the paste with a diluted surfactant. Mechanical aeration is more commonly employed in commercial applications,

as it allows for better control over the formation of smaller, more stable bubbles, thereby facilitating the regulation of the final properties of foamed concrete [42,43].

In this study, the influence of foaming agents and foam stabilizers (including recycled industrial oil as an eco-friendly alternative to traditional stabilizers) on the stability of the prepared foam, the pore structure, and the macroscopic properties of foamed concrete incorporating recycled additives (ground bricks as a form of recycled construction waste) was determined. Moreover, the suitability of these mixtures on the structural integrity and stability for application in additive manufacturing technologies was investigated. The use of these recycled additives presents the potential to reduce reliance on raw materials, lower production costs, and minimize the environmental impact of concrete production. By optimizing foam stabilization techniques and integrating recycled materials, this research aims to enhance the performance and sustainability of foamed concrete in large-scale 3D printing applications. The results will contribute to the development of cost-effective, environmentally friendly building materials and promote a circular economy and sustainability within the construction industry.

2. Materials and Methods

2.1. Designing the Mixture and the Method of Introducing Foam

Figure 1 presents a schematic overview of the process for developing new mixtures [44–47]. The research and production of lightweight foamed concrete incorporating recycled materials involve several key stages, each designed to ensure a systematic evaluation and optimization of the final product. The process begins with the preparation of the concrete mixture, during which recycled materials are introduced to the base mix. This stage is followed by the production of foamed concrete, accompanied by a simultaneous analysis of its properties. In parallel, the foam production and evaluation were carried out, with a particular focus on its stability, a critical parameter for the performance of foamed concrete. If the foam was found to be unstable, adjustments were made to its parameters or the mixing protocol as necessary. Nest, the design and production of a 3D printable foamed concrete (3DPFC) mixture are undertaken. During this stage, key parameters such as mixture density, the mortar-to-foam ratio, stabilizer concentration, and the water-to-cement ratio (maintained at 0.21) were determined. Once the mixture was prepared, its fresh properties were evaluated, including slump flow, setting time, and bulk density. When the foamed concrete achieves stability, it undergoes further testing to assess its shape retention and workability over time. If any of these properties failed to meet the required criteria, iterative adjustments were made to refine the process. Once all parameters were optimized, the buildability of the foamed concrete was tested through 3D printing at various intervals after mixture preparation. This step determines the material's suitability for additive manufacturing. The subsequent stage involves evaluating the hardened properties of the foamed concrete. This includes an assessment of shrinkage in printed elements, water absorption, and capillary rise. Moreover, the pore structure was analyzed, focusing on pore morphology, diameter range, and size distribution in the examined samples. This structured approach ensures a comprehensive evaluation of the quality and applicability of lightweight foamed concrete with recycled material additives for additive manufacturing, facilitating its potential adoption in sustainable construction practices.

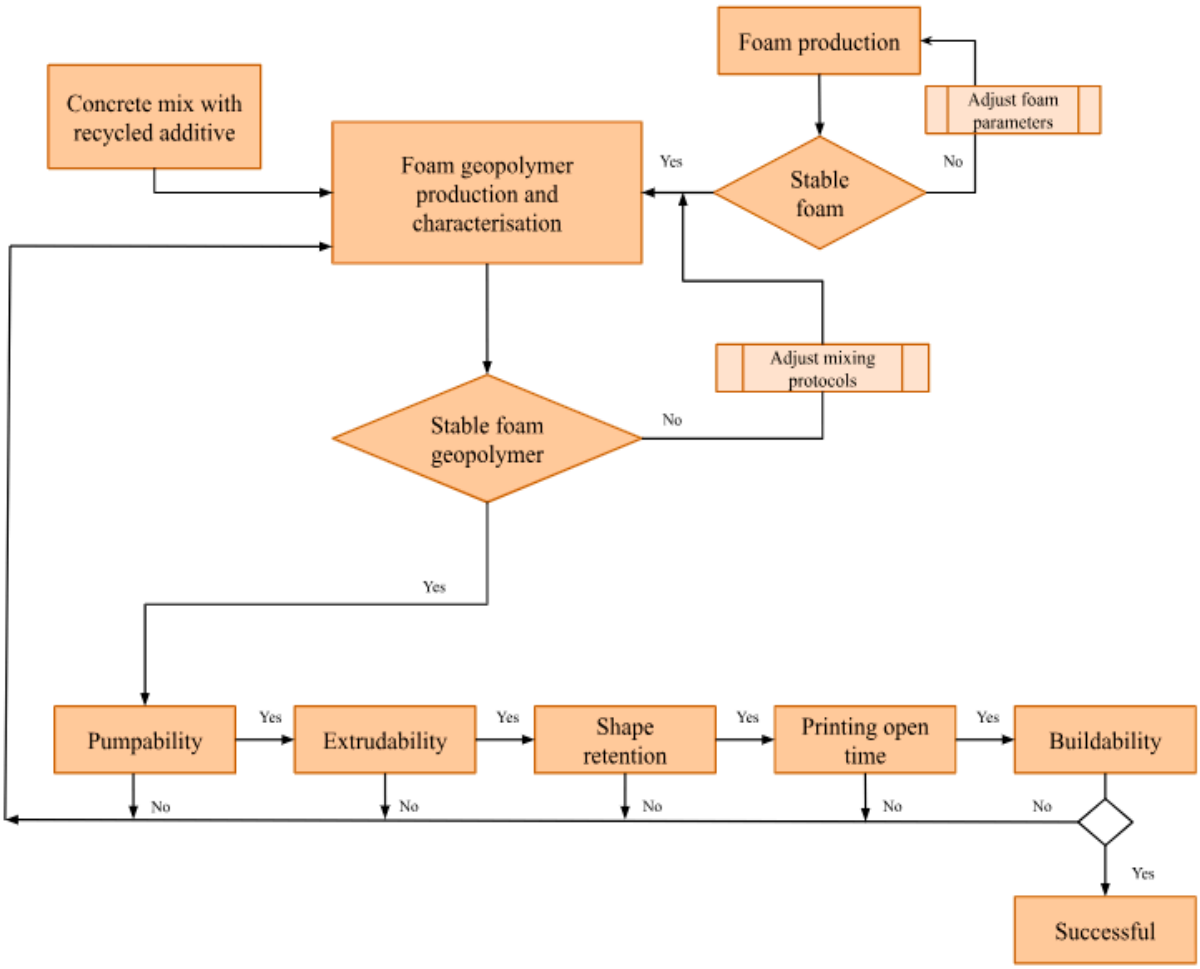


Figure 1. Flowchart of the procedure for developing new mixtures for 3D concrete printing applications.

2.2. Materials

The CEM I 52.5R ordinary Portland cement (OPC) supplied by Lafarge (Małogoszcz, Poland), quartz sand with a particle size range of 0.1–1 mm, ground brick (GB), and recycled materials were used to prepare the mixtures. The chemical composition of raw materials was determined using an EDX-7200 energy-dispersive X-ray fluorescence spectrometer, as shown in Table 1 (Shimadzu Corporation, Kyoto, Japan).

Table 1. Chemical composition of the raw materials.

Oxide Composition (%)	Material		
	Brick	**Sand**	**CEM I 52.5R**
CaO	1.23	1.20	59.91
SiO_2	60.1	81.50	27.76
Al_2O_3	15.7	13.01	4.05
Fe_2O_3	7.02	1.05	3.02
SO_3	-	-	3.55
K_2O	3.15	2.16	0.81
TiO_2	0.81	1.08	0.52
ZnO	-	-	0.03
MnO	0.10	-	0.13
SrO	-	-	0.08

Table 1. *Cont.*

Oxide Composition (%)	Material		
	Brick	Sand	CEM I 52.5R
V_2O_5	-	-	0.03
MgO	2.20	-	-
Na_2O	0.21	-	-
Cr_2O_3	-	-	0.02
ZrO_2	-	-	0.03
CuO	-	-	0.02
Rb_2O	-	-	0.01
Ir_2O_3	-	-	0.01
Y_2O_3	-	-	0.01
P_2O_3	0.16	-	-
Bi_2O_3	-	-	0.01

Two types of foaming agents were used, namely a synthetic foaming agent (PIANOTWÓR, AS) provided by MEEX-AG (Chrzanów, Poland) and a protein-based foaming agent (ISOCEM S/B, PS) supplied by ISOLTECH SRL (Verdellino, Italy). The basic properties of these foaming agents are presented in Table 2.

Table 2. The basic properties of foaming agents according to the manufacturers' data [48,49].

Component	Dosage (%)	Density (kg/m^3)	Compressive Strength After 7 Days (MPa)	Compressive Strength After 28 Days (MPa)
Synthetic Foaming Agent (AS)	2	1602	5.2	9.7
Protein-Based Foaming Agent (PS)	3	1600	5.5	10.1

To improve foam stability, two stabilizing additives were used, which were industrial machine oil (Orlen Velol RC 68, UO) supplied by Orlen Poland and a mixture of cetyl and stearyl alcohols (CAs) supplied by PCC Exol SA (Brzeg Dolny, Poland), whose properties are presented in Tables 3 and 4, respectively. The foamed concrete mixture design was developed through an in-depth review of the existing literature. This approach ensured a solid foundation in current knowledge and best practices. Additionally, the project aimed to verify the open time for 3D printing of a mixture incorporating ground brick as a supplementary material. The incorporation of crushed brick, a recycled waste material, introduces valuable reactive components, such as silica (SiO_2) and alumina (Al_2O_3), into the mix. These substances can improve the rheological properties of the concrete mixture and facilitate the cement binding process through pozzolanic reactions, which is crucial for enhancing the durability of the concrete and reducing its environmental impact. Research has shown that the addition of crushed brick in quantities ranging from 10 to 30% of the cement mass can enhance the mechanical properties of concrete, particularly in lightweight concretes with reduced density, while simultaneously lowering production costs and carbon footprint [50]. An important aspect in the design of foamed concrete mixes is the use of foam stabilizers, which help control porosity and foam durability during mixing. Industrial oil acts as a foam stabilizer by increasing the surface tension in the mixture, preventing the premature rupture of gas bubbles. This allows for better control of the pore structure, which is critical for achieving a homogeneous concrete structure with desired mechanical properties. Studies on lightweight foamed concrete have demonstrated that the inclusion of used oils improves foam durability and the uniform distribution of pores, contributing to the enhanced stability and mechanical properties of the material [51]. Additionally,

a mixture of cetyl and stearyl alcohols (CAs) used as a stabilizing agent reduces the surface tension of water, promoting the formation of smaller and more uniform pores in foamed concrete. This, in turn, enhances foam durability, particularly under intensive mechanical mixing. Examples of using fatty alcohols as foam stabilizers in lightweight concretes show their positive impact on the uniformity of pore structure and material stability, resulting in improved concrete quality. The development of a foamed concrete mix with the addition of crushed brick and foam stabilizers is based on strict control over the proportions of cement, crushed brick, water, and additives. The first step involves conducting preliminary tests to determine the impact of crushed brick on the rheological properties and strength of the mixture. Next, foam stabilizers are introduced to optimize the pore structure and ensure stability during mixing. The final stage involves validating the mix, with results including the evaluation of compressive strength, modulus of elasticity, and other functional properties, such as thermal and acoustic insulation. Research examples suggest that the inclusion of crushed brick and foam stabilizers in foamed concrete mixes can significantly improve the homogeneity of the material structure and its mechanical and thermal properties [52]. The foamed concrete mix with the addition of crushed brick and foam stabilizers represents a comprehensive approach that enables the production of concrete with desired properties. Through the use of these materials, it is possible to create lightweight, durable, and environmentally friendly concrete, which can be applied in various construction fields, including the production of structural elements such as tunnel covers and wall panels.

Table 3. Characteristics of the RC 68 guide oil.

Parameters	Unit	Typical Values
Kinematic viscosity at 40 °C	mm^2/s	69.5
Pour point	°C	−15
Flash-point	°C	230

Table 4. Characteristics of the EXOalc 1618 material.

Parameters	Unit	Analysis Result
Water content	(%)	0.3
Hydroxyl number	mgKOH/g	211
Iodine number	gJ2/100 g	<1.0

2.3. Foam Preparation

Foaming agents (AS) are chemicals incorporated into concrete mixtures to create and maintain a porous structure. These agents are widely used due to their effectiveness and ability to regulate pore quantity and size. This control is crucial for achieving the desired mechanical and insulating properties of the material. Moreover, synthetic foaming agents are characterized by high chemical stability, which contributes to the long-term durability of the material, improving the foamed concrete production process. However, a notable disadvantage of synthetic foaming agents is their higher cost compared to natural alternatives, as well as their potentially lower environmental friendliness. Protein-based foaming agents, on the other hand, are natural substances used to produce foamed concrete. For instance, the ISOCEM S/B agent, utilized in testing, is a highly effective foaming agent derived from a hydrolyzed protein of animal origin (from animal horns and hooves). These agents are particularly valued for their biodegradability and sustainable sourcing. However, they exhibit lower chemical stability relative to synthetic agents and present challenges in precisely controlling the size and distribution of pores. The choice of foaming agent significantly influences the mechanical, thermal, and insulating properties of foamed

concrete. For example, foaming agents can reduce the density of the material, which typically leads to a decrease in compressive strength. However, optimal formulations and proportions can mitigate this effect. Foamed concretes using synthetic foaming agents often display superior mechanical properties compared to those produced with protein-based agents, primarily due to the more uniform pore structure achieved with synthetics. Both types of foaming agents contribute to enhanced thermal and acoustic insulation properties of foamed concrete by increasing porosity, which improves overall insulating performance.

Foamed concrete incorporating protein-based foaming agents offers enhanced ecological and sustainability benefits, making it particularly advantageous in the context of sustainable construction. The addition of foaming agents also significantly influences the rheological properties of the mixture, which is critical for applications such as 3D printing. Excessive amounts of foaming agents can compromise the stability of printed structures; therefore, optimizing both the type and dosage of foaming agents is essential to achieve high-quality 3D printed foamed concrete. In the study of foamed concrete production, foam stability is commonly evaluated by monitoring its disintegration over time. This is typically performed using a transparent measuring cylinder; in the present research, 1000 mL polypropylene (PP) in a beaker with a handle was used for this purpose. Measurement of the volume of water separated from the foam is crucial for assessing foam stability and, if necessary, adjusting the foam-to-cement paste ratio. Figures 2 and 3 illustrate the temporal breakdown of the foam. The air pressure influenced the quality of the foam. Their increase from 4.0 to 6.0 bar accelerated the foam disintegration. Moreover, increasing the foaming agent concentration from 2% to 5% significantly enhanced foam stability (Figures 2 and 3). These results indicate the importance of optimizing parameters during foam production and selecting the appropriate water-to-foaming-agent ratio. The primary parameters influencing foam quality include the type and concentration of the foaming agent in the solution, air pressure, nozzle size, and ambient temperature. Detailed investigations of these parameters are necessary to ensure the production of high-quality foamed concrete with consistent and reliable properties.

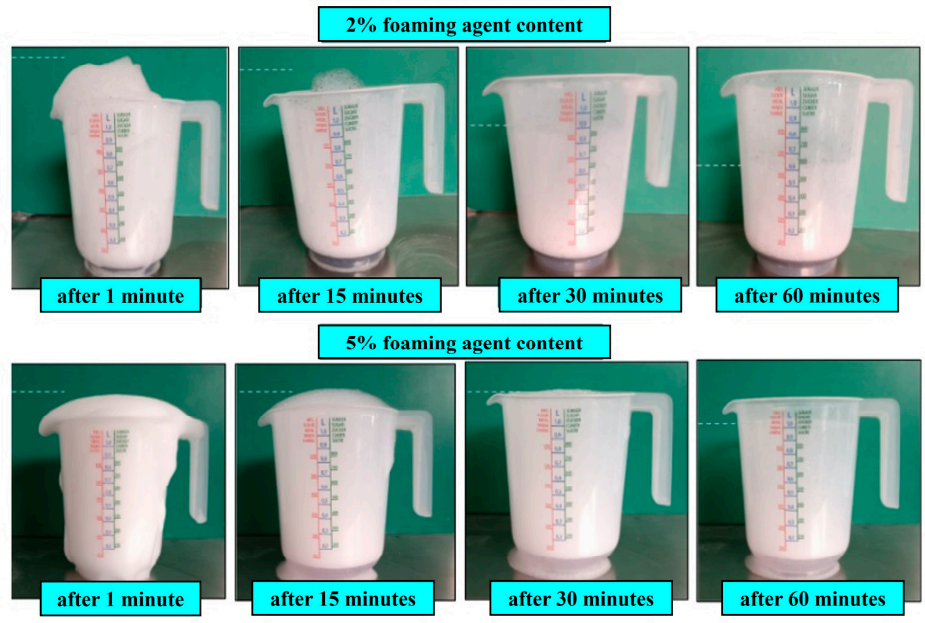


Figure 2. Foam stability at various synthetic foaming agent concentrations.

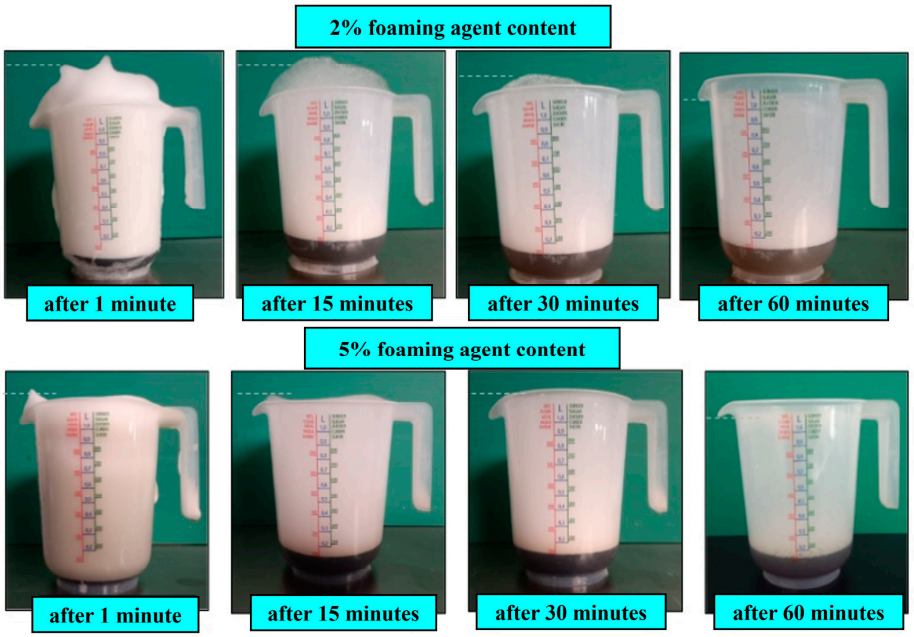


Figure 3. Foam stability at various protein-based foaming agent concentrations.

The protein-based foaming agent initially produces a higher volume of foam compared to foam generated with the synthetic agent. Moreover, it exhibits a faster rate of degradation. However, an increased concentration of both synthetic (AS) and protein-based (PS) foaming agents enhances foam stability over prolonged periods.

2.4. Process of Preparing the Mixture

The foamed concrete mixtures were formulated using cement, quartz sand, tap water, foaming agents, and foam-stabilizing additives. Six distinct mixtures were prepared, each differing in the combination of foaming agents and foam stabilizers. Reference mixtures were produced without the inclusion of foam stabilizers, while the experimental mixtures incorporated 1% by weight of RC 68 oil (UO), commonly utilized in industrial machinery, or a commercially available stabilizer, EXOalc 1618 (CA). In all mixtures, the proportion of foaming agents was maintained at 5% by weight relative to the total weight of the concrete mix, which included ground waste brick as a recycled additive. A consistent water-to-cement (w/c) ratio of 0.21 was applied across all formulations, accounting for the water introduced via the foaming agents and stabilizer. Detailed proportions of the mixture components are presented in Table 5.

Table 5. Compositions of foamed concrete mixtures with their designation.

No.	Mixture Designation	W/S	OPC (kg)	GB (kg)	Sand (kg)	UO (kg)	CA (kg)	PS (kg)	AS (kg)
1	M1	0.21	1.6	0.5	2.9	-	-	0.25	-
2	M2	0.21	1.6	0.5	2.9	-	-	-	0.25
3	M3	0.21	1.6	0.5	2.9	0.05	-	0.25	-
4	M4	0.21	1.6	0.5	2.9	0.05	-	-	0.25
5	M5	0.21	1.6	0.5	2.9	-	0.05	0.25	-
6	M6	0.21	1.6	0.5	2.9	-	0.05	-	0.25

2.5. Methods

2.5.1. Stability and Consistency of Foam and Foamed Concrete

The quality of the produced foam was evaluated as an initial step in the study. The prefabricated foam was generated using a BP-4041 pneumatic foam gun (BASS POLSKA, Mroków, Poland) with a capacity of 25 L. Adjustments to foam characteristics can be achieved by modifying several parameters, including the air pressure (operating range: 4–5 bar), the size and type of the nozzle, and the pore size of the membrane integrated into the lance of the device.

The preparation of test mixtures of foamed concrete was carried out using a Clatronic KM 3765 slow-speed planetary mixer (CTC Clatronic Sp. z o.o., Opole, Poland) equipped with a 1500 W motor and a 10 L capacity bowl, ensuring both reliability and operational efficiency. The mixing speed was maintained within the range of 58–220 rpm, an optimal setting to achieve a uniform mixture consistency without compromising the integrity of the air bubbles formed within the mixture.

The consistency of the concrete mixtures was evaluated in accordance with the PN-EN 12350-5 standard [53], which specifies the flow spread measurement of the concrete on a flat, vibrated surface.

2.5.2. Buildability

The idea for the design solution was developed as part of an "implementation doctorate". The tests carried out allowed for the development of the solution used in the research. The 3D printing device operating in gantry mode was used. The equipment featured a printing volume of 1000 mm (X-axis), 500 mm (Y-axis), and 500 mm (Z-axis), with a maximum head travel speed of 80 mm/s. The printing head was equipped with a 20 L material hopper, incorporating a constant-pitch screw feeder with a length-to-diameter ratio of 3.5. Material extrusion was facilitated through a nozzle with a 20 mm diameter round orifice. The layer height was set to 8 mm with a line width of 20 mm. During the experiment, the foamed concrete mixture was simultaneously cast into rectangular cuboid molds (40 × 40 × 160 mm) for comparative analysis. The printing speed for each layer was maintained at 40 mm/s, resulting in an extrusion rate of approximately 6400 mm^3/s. For each material, two parallel lines were printed in a five-layer configuration, producing samples measuring 40 × 40 × 480 mm. After curing, the printed samples were cut to the required dimensions for strength testing. The results were then compared with those obtained from samples of analogous compositions that had been cast into molds, allowing for a direct assessment of the mechanical performance of the two production methods.

2.5.3. Apparent Density

The printed samples were cured in air at an ambient temperature of 22 ± 2 °C and a relative humidity (RH) of 55%, reflecting typical construction site conditions. After a curing period of 14 days, the external dimensions (height and diameter) and the weight of the samples were measured to determine their bulk density prior to compressive strength testing. Bulk density, defined as the ratio of the material's mass to its total volume (including pores), was calculated using Formula (1):

$$Pp = \frac{m}{V} \quad (1)$$

where m—mass of the sample; V—volume of the sample.

2.5.4. Capillary Water Absorption

For testing the capillary water absorption of foamed concrete samples, specimens were placed in containers filled with water, supported on plastic grids to ensure separation from the bottom of the vessel. This setup allowed the water-absorbing surface to correspond to the base area of the sample, calculated as 1600 mm^2. The samples, fabricated using both 3D printing and casting methods, were uniformly sized at 40 × 40 × 160 mm.

The absorption process was monitored by periodically weighing the samples using a precision scale with an accuracy of 0.01 g, enabling detailed tracking of mass changes. During the initial phase of rapid water uptake, measurements were performed at short intervals—every 1, 2, or 4 h. As the rate of absorption decreased, the weighing intervals were extended to every two days. Throughout the test, the water level was maintained at a depth of 2–3 mm to ensure consistent conditions.

Figure 4 depicts the experimental setup for water absorption testing, performed in both vertical and horizontal orientations. In the vertical orientation (1), the test followed standard engineering principles to evaluate capillary water absorption through the height of the sample. Conversely, in the horizontal orientation (2), the test aimed to assess potential differences in water absorption across the layers of the 3D printed samples. This distinction is particularly relevant, as the layer-by-layer deposition in 3D printing can result in structural variations that may influence water absorption behavior.

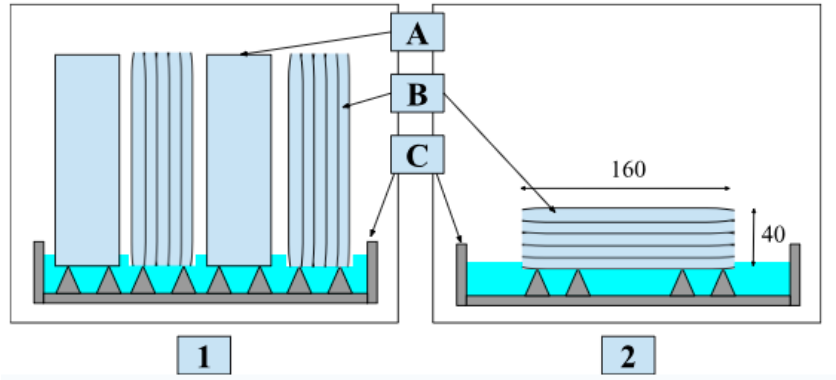


Figure 4. Scheme of capillary water absorption test illustration. A—foam concrete tube; B—foamed 3D printed sample; C—capillary tray; 1—vertical orientation; 2—horizontal orientation.

The water absorption coefficient A was calculated according to Formula (2):

$$A = \frac{\Delta m_t}{F \times \Delta\sqrt{t}}, \quad (2)$$

where

A—water sorption coefficient, ($kg/(m^2h^{1/2})$);
Δm—sample mass increase, (kg);
F—suction surface, (m^2);
$\Delta\sqrt{t}$—time square root increase, ($h^{1/2}$).

Moreover, the water sorption phenomenon was analyzed by using the FLIR E96 thermal imaging camera (Teledyne FLIR, Wilsonville, OR, USA), recording photos in 5 min intervals for 120 min. This device is used for the non-contact measurement of infrared radiation emitted by object surfaces.

2.5.5. Microscopy Observation

A Techrebal Banito B2920 digital microscope (Techrebal, Wilczyce, Poland), equipped with 100× magnification and a built-in 48MP camera, was used for microscopy analysis. The pore structure of foamed composites was examined to evaluate the impact of the foaming agent and the manufacturing method (3D printing vs. casting) on pore shape, size, and packing density. The acquired images were analyzed using Fiji ImageJ IJ 1.46r.

2.5.6. Flexural Strength Tests and Compressive Strength Tests

Mechanical strength tests were performed using the MTS Criterion 43 testing machine (MTS Systems, Eden Prairie, MN, USA) in conjunction with MTS TestSuites 1.0 software. Test specimens measuring 40 × 40 × 160 mm were prepared for the analysis. Flexural strength tests followed the PN-EN ISO 178 standard [54], with a testing speed of 5 mm/min, where each specimen was supported at two points spaced 100 mm apart.

Compressive strength tests adhered to the EN 12390-3 standard [55], utilizing samples with dimensions of 40 × 40 × 40 mm and tested at a speed of 1 mm/min. These standardized methodologies ensured accurate and reliable results, providing a robust assessment of the material's mechanical performance for practical applications.

3. Results and Discussion

3.1. Consistency and Density Characteristics of Foamed Concrete

The evaluation and understanding of the consistency of a foamed mixture prior to initiating 3D printing are critical, as the consistency directly influences the precision and quality of the printed structure. An optimal consistency ensures that the material retains its properties and stability during the layer-by-layer application process. A mixture with excessive fluidity can lead to spillage and loss of print shape, whereas an overly viscous one may result in flow challenges and application difficulties. Moreover, consistency also plays a crucial role in the adhesion and bonding of the mixture, which are fundamental for the structural integrity of the final object. Proper consistency ensures effective bonding between individual layers, thereby contributing to the durability and stability of the printed structure. Furthermore, understanding the consistency of the mixture facilitates adjustments to printing parameters, such as extrusion speed and temperature, which optimize the process and reduce the risk of defects. The bubble quantity and structure within the foam significantly impact the stability of the lower layers during printing. Over time, foam instability may arise due to bubble coalescence driven by pressure differences [56]. To investigate these phenomena, the stability of the fresh composite foam was analyzed both before and after extrusion, as well as over time. Wet density measurements were used to assess the stability of the mixtures. These measurements provide direct insights into foam stability in aerated concrete; an increase in density indicates foam collapse within the composite material [57]. This evaluation highlights the dependence between consistency, foam stability, and printing parameters, which collectively determine the success and quality of 3D printed foam-based materials. Figure 5 presents the temporal changes in the density of the studied mixtures, providing insights into the stability of foamed concrete. For samples incorporating synthetic foaming agents, M1 exhibited a relatively stable increase in density, from 3.3% after 30 min to 4.1% after 180 min. This indicates moderate foam stability, with more pronounced changes occurring after the initial 30 min attributed to foam degradation processes such as liquid expulsion, gas diffusion, and liquid film rupture, as described in the literature [58]. Phenomena such as liquid expulsion from the foam, gas diffusion, and liquid film rupture significantly impact the stability of foamed concrete. Liquid expulsion due to gravity and surface tension reduces the film thickness, leading to rupture [59]. Moreover, gas diffusion contributes to bubble coalescence, further destabilizing the foam structure.

The behavior of M3 revealed exceptional foam stability, as evidenced by a negligible density decrease of 0.1% after 180 min. Similarly, M5 demonstrated good foam durability, with a minimal density increase of 0.7% over the same period, indicating minimal structural changes over time. For mixtures with protein-based foaming agents, M2 shows a stable yet modest density increase, ranging from 0.6% after 30 min to 1.6% after 180 min, reflecting relatively stable foam properties. In contrast, M4 displayed the most significant density increase, rising from 4.1% after 30 min to 5.6% after 180 min, indicative of considerable foam degradation and instability over time. M6 showed a moderate density increase, from 1.3% after 30 min to 2.44% after 180 min, suggesting moderate foam stability with a tendency for gradual deterioration. The results indicate that most samples, except for M4 and M6, experienced a slight decrease in density within the initial 15 min, which stabilized thereafter. The initial decrease in density observed in foamed mixtures can be attributed to foam settling and the rearrangement of air bubbles within the matrix. During this phase, air redistributes within the foam structure, resulting in a more uniform configuration and a temporary reduction in density. Furthermore, the burst of larger air bubbles contributes to a decrease in air content, which leads to increases in the density of the mixture. Following this preliminary stage, as the foam structure stabilizes, density begins to rise again. This increase may be linked to the progressive binding of the material and tightening of the foam matrix during which the air content becomes fixed and stable. The consistency of the mixture significantly affects not only the mechanical properties of the final product, such as strength and durability, but also its esthetic attributes by mitigating issues like surface unevenness or cracking. Another critical parameter is the open time of the foamed mixture, defined as the duration during which the material remains workable before curing initiates. Knowledge of the open time enables effective planning of the printing process, ensuring the material is applied during its optimal workability period. An inadequately short open time may cause application challenges, such as clogging of the material in the nozzle and failure to achieve the desired properties in the printed structure. To evaluate the time at which the mixture achieves a consistency suitable for 3D printing, a slump test was performed using the slump table method [58–60]. The obtained results are presented in Table 6.

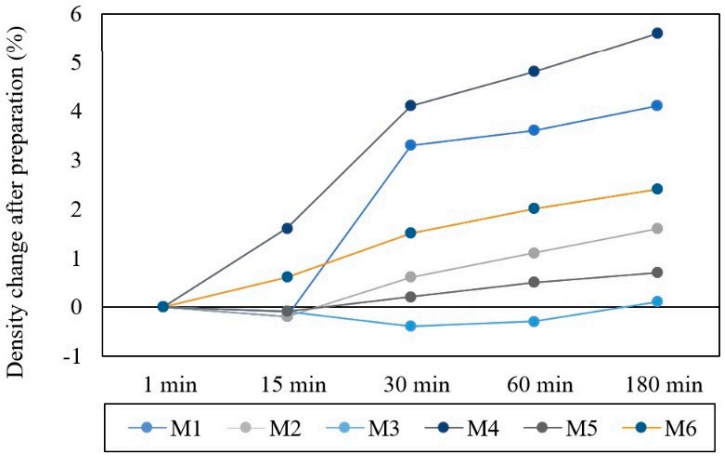


Figure 5. Percentage increase in density of the tested mixtures as a function of time.

The results of the consistency study indicate that the time required to initiate the printing process varies depending on the type of foaming agent used. Figure 6 presents the optimal parameters for each mixture, determined based on the consistency of the foamed concrete before and after performing the slump test. The slump test results reflect both the mixture's buildability and its ability to retain shape, which are critical factors for successful 3D printing applications.

Table 6. Flow characteristics of mixtures as a function of time from preparation, according to PN-EN 1015-3.

Mixture Designation	Flow Diameter (mm) Time from Preparation (min) 1	15	30
M1	180	160	150
M2	170	140	120
M3	160	140	120
M4	145	130	115
M5	145	125	110
M6	140	120	110

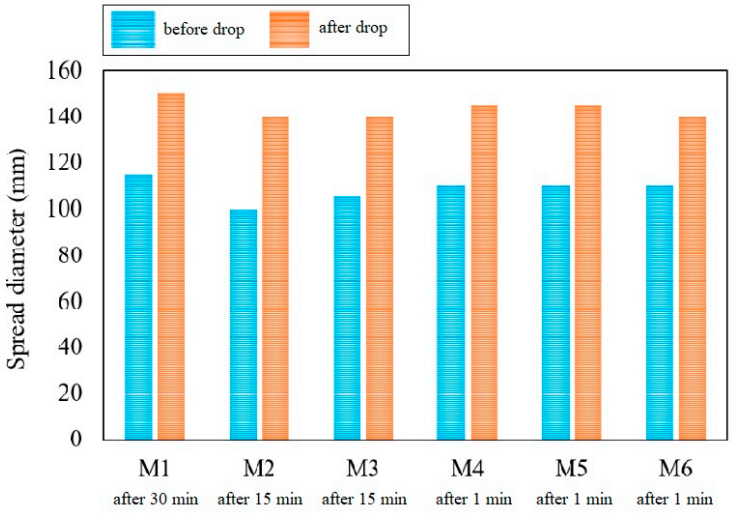


Figure 6. Flow diameters of fresh foamed concrete.

Additional studies were conducted, incorporating both microscopic and macroscopic analyses of the foam to evaluate its degradation time in relation to the type of stabilizer utilized. The microscopic analysis offered a detailed perspective on structural changes at the cellular level, enabling the observation of air bubble size and morphology over time. Concurrently, the macroscopic analysis facilitated the evaluation of overall foam stability and volumetric loss under controlled conditions. By integrating these methodologies, the research sought to elucidate the influence of different stabilizers on the durability and structural integrity of the foam, providing a comprehensive understanding of their effectiveness in enhancing foam stability. The presented images illustrate the foam degradation process under different conditions and with the application of various stabilizers over time (1 min, 15 min, and 30 min after preparation).

For AS foam (Figure 7), in the absence of a stabilizer (a), rapid degradation is observed. After 15 min, a significant reduction in both bubble size and number is evident, and after 30 min, the foam is almost completely degraded. The introduction of the UO stabilizer (b) substantially improves foam stability—bubbles persist in greater numbers and for a longer duration. However, an increase in bubble size over time is observed, which may indicate coalescence. The application of the CA stabilizer (c) also enhances foam stability compared to the sample without a stabilizer, although its effectiveness is lower than that of UO. Smaller bubbles and moderate degradation over time are evident. For PS foam (Figure 8), the sample without a stabilizer (a) demonstrates rapid structural collapse of the foam. The UO stabilizer (b) significantly increases foam durability, maintaining the bubble structure to a much greater extent, with degradation occurring at a much slower rate compared to the unstabilized sample. Similarly, the CA stabilizer (c) improves foam stability during the observation period (30 min), with air particles showing minimal degradation.

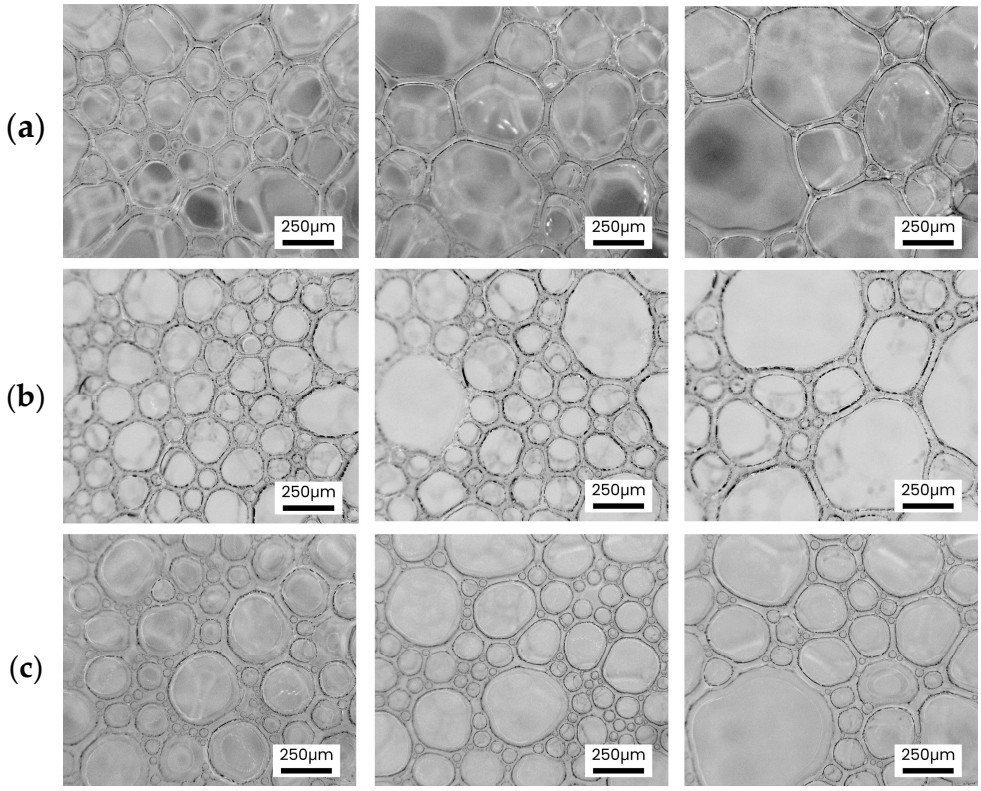


Figure 7. Foam degradation from (left) 1 min after preparation, after 15 min, and after 30 min on the right; (**a**) AS without stabilizer, (**b**) AS with UO, (**c**) AS with CA.

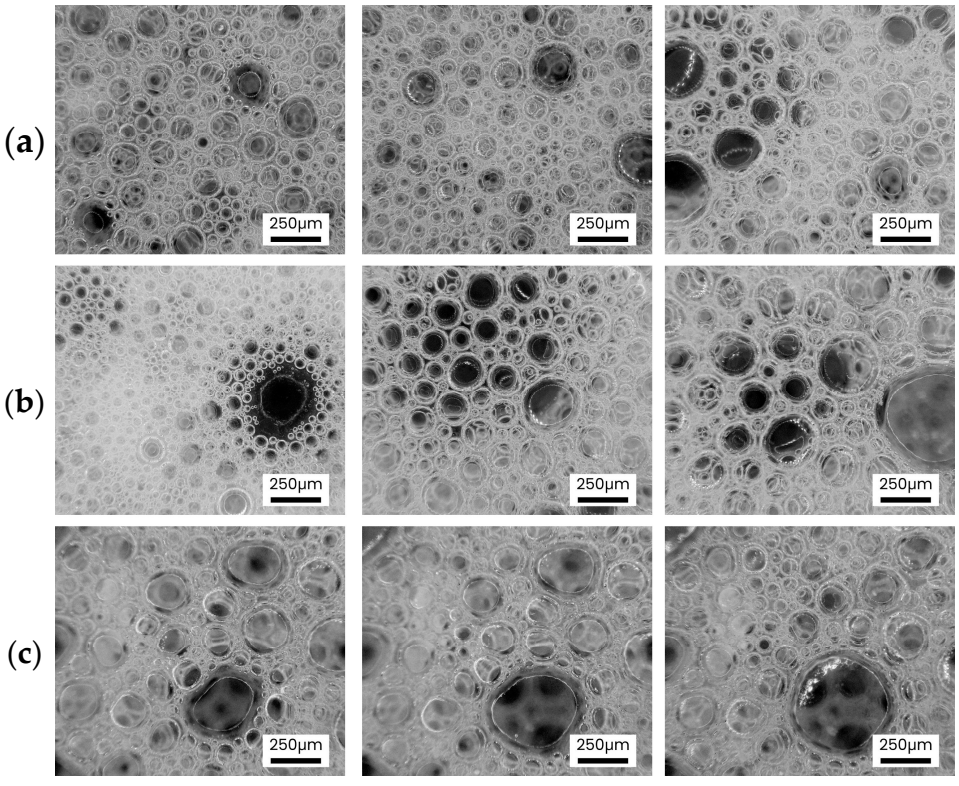


Figure 8. Foam degradation from (left) 1 min after preparation, after 15 min, and after 30 min on the right; (**a**) PS without stabilizer, (**b**) PS with UO, (**c**) PS with CA.

3.2. Buildability

To evaluate the extrudability of cellular concrete mixture, five individual layers, each 490 mm in length, were printed for each composition under consistent feed rates and printing speeds. Extrudability was considered satisfactory if the layers were printed successfully without variations in thickness, cracks, delamination, or blockages. Buildability was assessed by examining the deformation of the lower layers under the weight of subsequent layers. Uniformity in layer thickness along the layers' length was deemed essential. Additionally, the mixture was required to demonstrate sufficient flexibility and stability to prevent cracking during extrusion while minimizing the risk of delamination, which could compromise the structural integrity of the printed element [61–64]. To ensure efficient and smooth printing operations, the material must exhibit unobstructed flow through the nozzle, facilitating continuous extrusion [65]. During the deposition of successive layers, the mixture should retain its shape after printing, while the underlying layers must resist excessive deformation under the weight of additional layers [66]. Structural stability is vital to enable subsequent layers to support the imposed loads and maintain their geometry throughout the construction process. Moreover, achieving uniform bonding between layers is essential to ensuring the overall structural integrity and mechanical strength of the final product. Adherence to these criteria is critical for fabricating a durable, well-constructed structure with satisfactory mechanical performance. The printing process for the evaluated mixtures is illustrated in Figure 9.

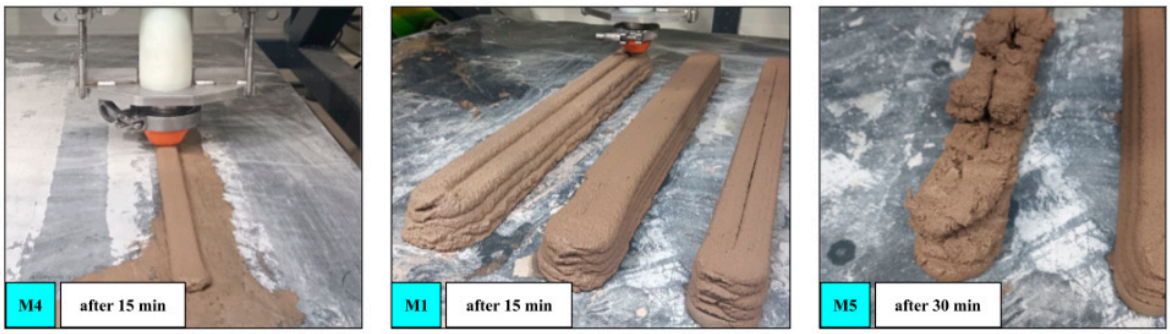


Figure 9. Printing process using mixtures of varying compositions and consistencies at different time intervals after preparation.

Based on the observations presented in Figure 9, several conclusions can be drawn regarding the consistency and temporal stability of foamed concrete mixtures. The mixture incorporating PS demonstrated superior shape retention and structural stability over time compared to those containing AS. This indicates that PS agents enhance the resistance of the mixtures to deformation under sustained conditions. Furthermore, the inclusion of stabilizing agents also had a significant impact on the structural integrity and shape retention of the printed layers. The mixture without stabilizers (M1) exhibited pronounced deformation and sagging over time, even after just 30 min, highlighting insufficient foam stability. In contrast, the mixture incorporating UO as a stabilizer (M4) showed improved shape retention after 15 min, outperforming mixtures without stabilizers. However, the addition of CA as a stabilizer (M5) rendered the mixture unsuitable for printing after 30 min. For this additive, the open time for printing should not exceed 20 min after preparation, which poses challenges for on-site applications and large-scale printing processes. Samples incorporating synthetic foaming agents (M1, M3, M5) exhibited notable challenges in terms of extrusion quality and buildability. The sample without a stabilizer (M1) displayed an irregular structure with prominent cracks and gaps between layers, indicating instability of the material during extrusion. The layers failed to maintain a uniform shape, resulting

in significant deformations, particularly in the lower sections. The sample containing UO (M3) demonstrated improved control over layer thickness compared to M1; however, imperfections persisted at the layer junctions (Z-seams), and minor unevenness was observed. Despite these issues, delamination was not evident, and the sample retained its shape with reduced deformations relative to M1. The sample with used oil and CA (M5) exhibited a denser consistency and a rough surface finish. The addition of stabilizers in this mixture significantly reduced the open time, rendering the material unprintable after 30 min post-preparation (Figure 10, M5). In contrast, samples with protein-based foaming agents (M2, M4, M6) demonstrated markedly superior extrusion and build quality, aligning with findings reported in the literature [67,68]. The sample without a stabilizer (M2) demonstrated good extrusion quality, although minor defects were observed at the layer interfaces. Despite these imperfections, the construction retained its shape without significant deformations, indicating satisfactory buildability. In the mixture containing UO (M4), the layers exhibited uniformity and strong bonding, with no visible interruptions, highlighting the material's stability during printing. Sample M6, however, faced some challenges in extrudability, including unevenness and interruptions in the printed layers. Despite these issues, the structure maintained overall stability, though with slightly greater deformations compared to M2. Figure 10 illustrates the stacked layers of the printed foamed mixtures, providing a visual evaluation of buildability by comparing the deformation of the lower layer. The images reveal areas of minor deformation, with arrows marking locations where the lower layer was damaged during the removal of the print from the printer bed. This damage was attributed to the application of pressure on the brittle and delicate material. It is important to note that assessing buildability using five stacked layers may not fully capture the failure criteria relevant to precast construction elements, where larger-scale and more complex geometries could influence structural performance.

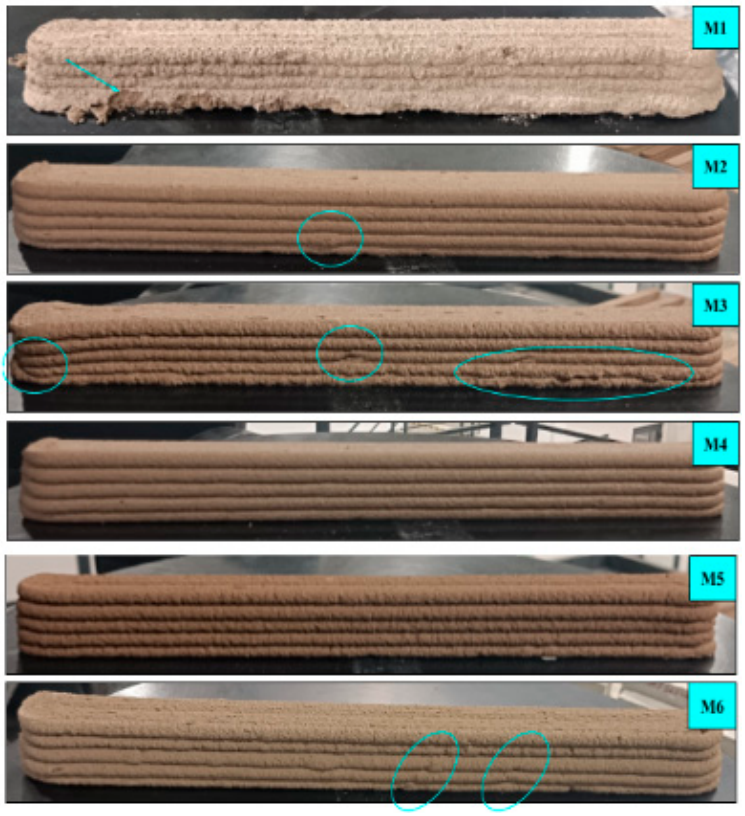


Figure 10. Buildability of printed foam concrete using mixtures of varying compositions and consistencies.

Figure 11 presents a comparative analysis of the extrudability and buildability of foamed concrete samples produced with synthetic (M1, M3, M5) and protein-based (M4, M2, M6) foaming agents, alongside the effects of foam stabilizers. The images highlight differences in layer deposition quality (Z-seam), structural stability, and surface smoothness between the two types of foaming agents. Arrows indicate regions where a noticeable sagging of layers occurred due to the weight of the overlying material. The sample M1, printed 30 min after mixture preparation, exhibited significant flow and deformation in the lower layers, compromising structural stability. In contrast, the freshly prepared sample M3 demonstrated an uneven surface at the Z-seam; however, the front view revealed uniformly deposited and stable layers. For sample M6, it was observed that the three lower layers are visibly wider than the upper layers. This effect is likely attributed to the rapid action of the stabilizer, which affected the consistency of the mixture during extrusion, leading to changes in layer geometry over the printing process.

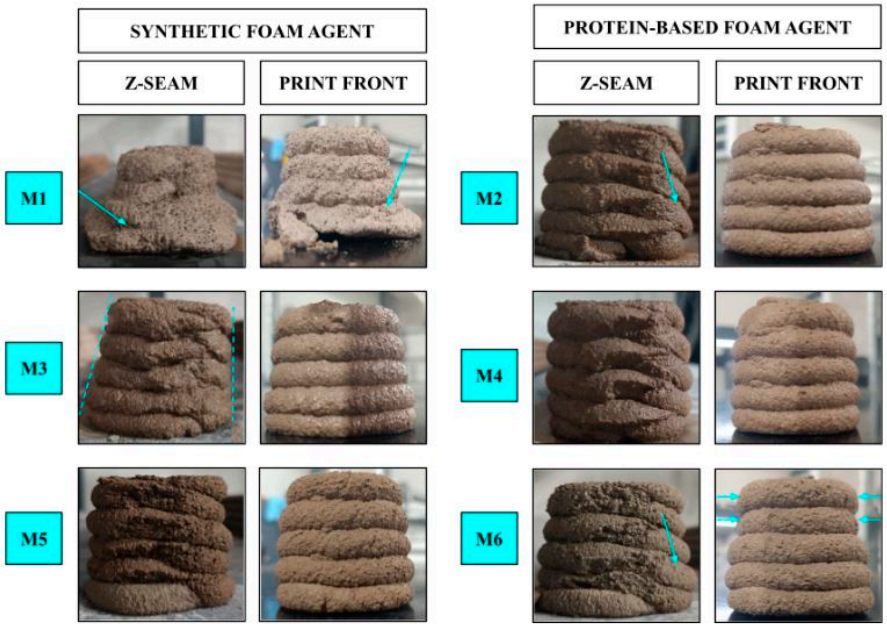


Figure 11. Comparison of the extrudability and buildability of foamed concrete samples produced with synthetic foaming agents (M1, M3, M5) and protein-based foaming agents (M4, M2, M6).

3.3. Apparent Density

The analysis of the production method's impact on apparent density, as presented in Figure 12A, reveals that cast samples exhibit lower density compared to those produced via 3D printing. The density differences range from 0.2 to 0.5 g/cm^3, indicating that 3D printed samples are denser and more stable. This observation is consistent with the inherent characteristics of the 3D printing process, which involves layer-by-layer extrusion, leading to the natural densification of the material [69]. This method ensures effective space filling while reducing the number of pores, thereby contributing to increased density. The smallest percentage differences in density between printed and cast samples were observed in mixtures M5 and M6 containing the CA stabilizer, with difference values of 6% and 11%, respectively. This phenomenon can be attributed to the rapid initiation of binding and emulsification processes in these mixtures, enabling them to retain their foaming parameters across both casting and printing techniques. This outcome is particularly advantageous in 3D printing, as successive layering does not significantly compromise the pore structure, thereby preserving the material's insulating properties. Stabilization, in terms of maintaining the density of foamed materials, enhances the control over the 3D printing process and contributes to material efficiency. Furthermore, the apparent

density results were classified to examine the influence of stabilizers on material properties for different production methods. Figure 10 illustrates that the application of stabilizers significantly improves material stability. Samples without stabilizers exhibited the lowest density and were less stable, as shown in Figures 10 and 11, making them unsuitable for applications requiring long-term durability [70–72]. The incorporation of the used oil stabilizer (UO) results in a slight increase in density, enhancing stability. However, the most significant improvement in sample density was observed with the addition of the CA stabilizer (EXOalc 1618), which led to a substantial increase in material density, indicating an enhancement in material structure. This, however, also results in a higher mass of samples. A potential compromise could involve the use of a moderate amount of CA stabilizer, maintaining adequate stability while achieving an acceptably low density. This presents an excellent opportunity for further research to optimize the proportion of ingredients, thereby improving the material's properties. Future studies could also focus on understanding the mechanisms influencing the binding and stability of foamed concrete under various technological conditions, particularly at larger scales. Figure 12C highlights the influence of foaming agent type on concrete density. Samples produced with synthetic foaming agents (AS) exhibit lower apparent density, ranging from 1.46 to 1.90 g/cm^3, which is advantageous in terms of material weight reduction. In contrast, concrete produced with protein-based foaming agents (PS) shows a broader density range, from 1.06 to 2.05 g/cm^3. While the increased density of PS samples may contribute positively to structural stability, the synthetic agent (AS) appears more suitable for optimizing lightweight foamed concrete. The addition of the CA stabilizer further contributed to reducing the density in both cast and 3D printed samples.

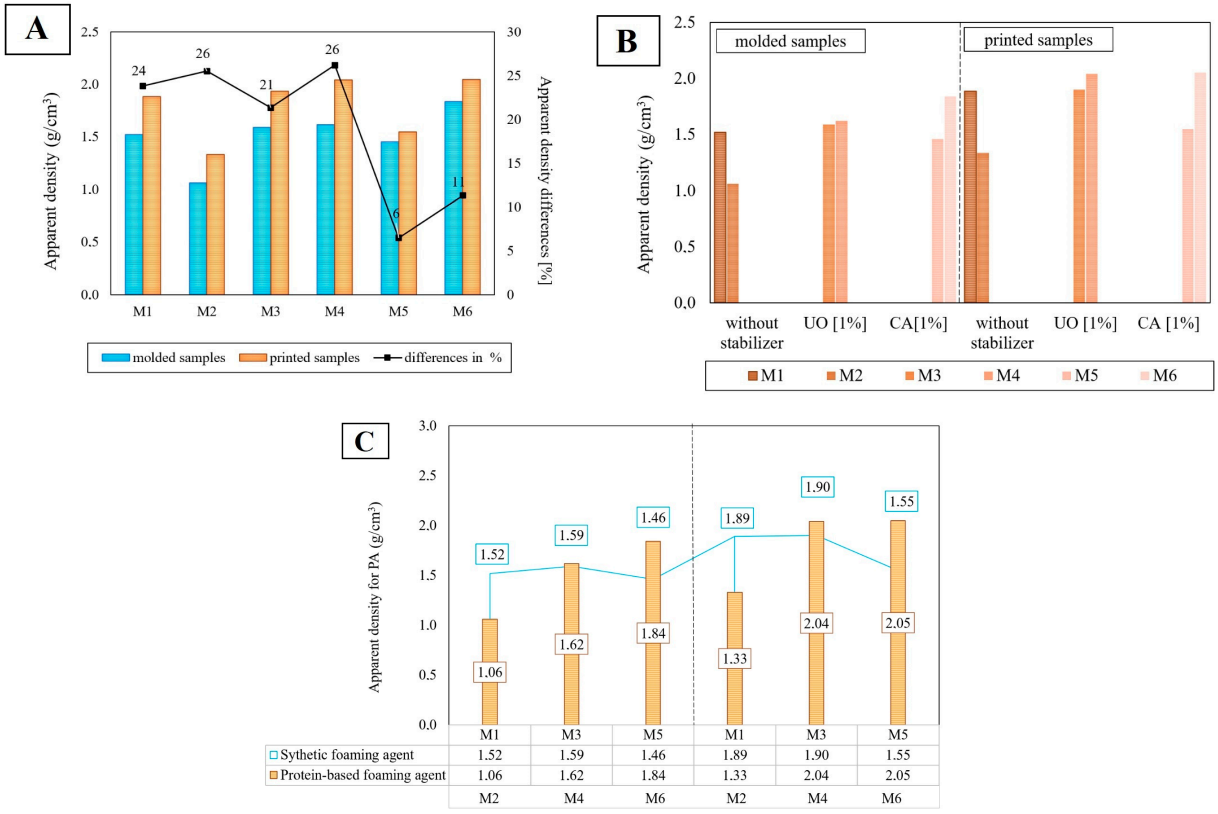


Figure 12. Variation in foamed concrete apparent density based on (**A**) production method, (**B**) stabilizer type, and (**C**) foaming agent.

3.4. Water Absorption

Figure 13 presents a view of the samples during the water absorption tests, concerning the influence of sample orientation and the type of mixture used. In contrast, Figure 14 depicts the relationship between water absorption and time for sample M1. The water absorption coefficient A was calculated for each sample.



Figure 13. View of the samples during water absorption concerning the influence of sample orientation and the type of mixture used.

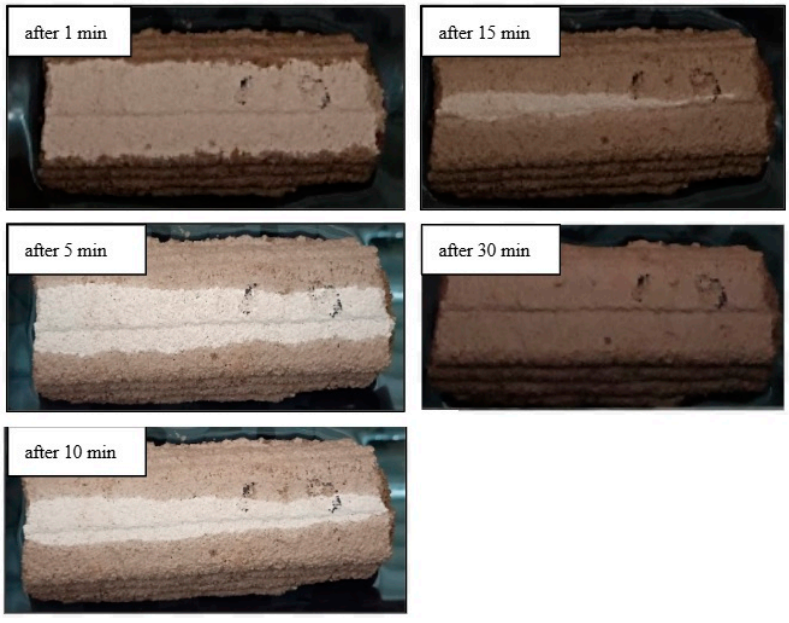


Figure 14. Water absorption of sample M1 over time.

The results presented in Figures 15 and 16 demonstrate differences in water absorption depending on sample orientation, mixture type used, and production method. Figure 15 shows the mass gain of the samples per unit area over time, while Figure 16 displays the calculated water sorption coefficients. For samples positioned vertically, corresponding to the standard method for assessing capillary absorption, mixture M1 (foamed with a synthetic agent without a stabilizer) exhibited the highest water absorption. This was char-

acterized by a rapid mass increase during the initial hours of the experiment, likely due to the high porosity and open structure of the sample, which facilitates intense water uptake. In contrast, mixtures M2 (foamed with a protein-based agent without a stabilizer), M3, M4, M5, and M6 demonstrated lower water absorption levels. Among these, samples M5 and M6, containing the CA stabilizer, exhibited the lowest water absorption, likely due to their denser concrete structure, which restricts water penetration. When the samples were oriented horizontally, a general trend of slightly reduced water absorption was observed compared to the vertically oriented samples, indicating the influence of orientation on water uptake behavior. These differences are particularly evident in mixture M1, where horizontal absorption reaches lower maximum values compared to the vertical orientation. This discrepancy is likely attributable to variations in the layered structure of the material produced via 3D printing, with layers potentially exhibiting differing absorption properties. This observation aligns with findings from other studies, which indicate that in samples oriented directed parallel to the horizontal axis in a coordinate system (*X*-axis), water rapidly infiltrates vertical interlayer spaces at the onset of the absorption process [73]. The graph of water sorption coefficients (Figure 16) indicates that mixture M1 achieves the highest coefficient value among the printed samples, measuring 1.9 $kg/(m^2 \cdot h^1/^2)$, indicating very intense water absorption. In contrast, the coefficients for the remaining samples are significantly lower. Mixtures M5 and M6, both stabilized with CA, exhibit the smallest sorption coefficients, confirming that stabilizers effectively reduce water permeability and flow through the material. Analyzing the results in conjunction with Figure 15, it is evident that samples with lower apparent density exhibit higher water absorption. For instance, sample M1, which has one of the lowest apparent densities (1.52 g/cm^3 for cast samples), demonstrates the highest water absorption in the graphs depicting capillary water uptake. Conversely, samples M5 and M6, containing the CA stabilizer, show higher apparent densities (up to 2.05 g/cm^3 for printed samples), correlating with lower water absorption. This indicates that lower apparent density is associated with increased material porosity, facilitating capillary water uptake, while higher apparent density reflects a denser concrete structure that restricts water penetration [74,75]. Furthermore, the consistency of the foamed concrete, defined by its ability to retain shape after extrusion through the 3D printer nozzle, influences its capillary properties. As shown in Figure 12, samples foamed with synthetic agents (M1, M3, M5) and exhibiting lower consistency tend to have a more uneven surface and pronounced Z-seam joints. These irregularities provide additional pathways for water infiltration, resulting in higher water absorption. In contrast, samples with a denser structure and improved extrudability, such as those foamed with protein-based agents (M2, M4, M6), exhibit a more uniform surface. This minimizes water penetration, as reflected by their lower water absorption values and higher apparent densities.

In the context of moisture studies, temperature differences between wet and dry areas allow for the visualization of regions with elevated water content. The moisture accumulating in the material typically has a lower temperature, which in our case appears as blue areas on the thermographic image compared to the dry sections, (Figure 17). The study confirms that sample M1 exhibits the highest water absorption with the largest, often interconnected, and irregular pores, as shown in Figure 18. Protein-based foaming agents show lower water absorption in samples without stabilizers (M2) and in samples stabilized with UO (M4) compared to those with synthetic foaming agents (M1 and M3). However, the samples stabilized with CA (M5 and M6) do not show significant differences after 120 min of immersion, which is consistent with the data presented in Figure 15. According to the section discussing optical microscopy, foamed samples using a protein-based agent feature smaller, more evenly distributed pores. This microstructure promotes a more uniform and compact pore network, which reduces the overall porosity of the material. In

concrete with large, irregularly distributed pores, these spaces easily connect to form larger capillary channels, facilitating rapid and extensive water absorption. Such a structure allows water to move more freely within the material, as the irregular pores create multiple pathways for flow. In contrast, in samples with small, regularly shaped pores and a uniform distribution, water encounters more resistance because the smaller and evenly distributed pores limit the formation of capillary pathways. As a result, concrete with a homogeneous microstructure exhibits significantly lower water absorption compared to concrete with large, irregular pores. Consequently, the reduced pore size and more uniform distribution limit the material's ability to absorb water, as fewer and smaller spaces are available for water penetration. This explains the lower water absorption observed in protein-based foamed concrete compared to samples with synthetic agents, where the pore structure may be less uniform and more prone to water uptake.

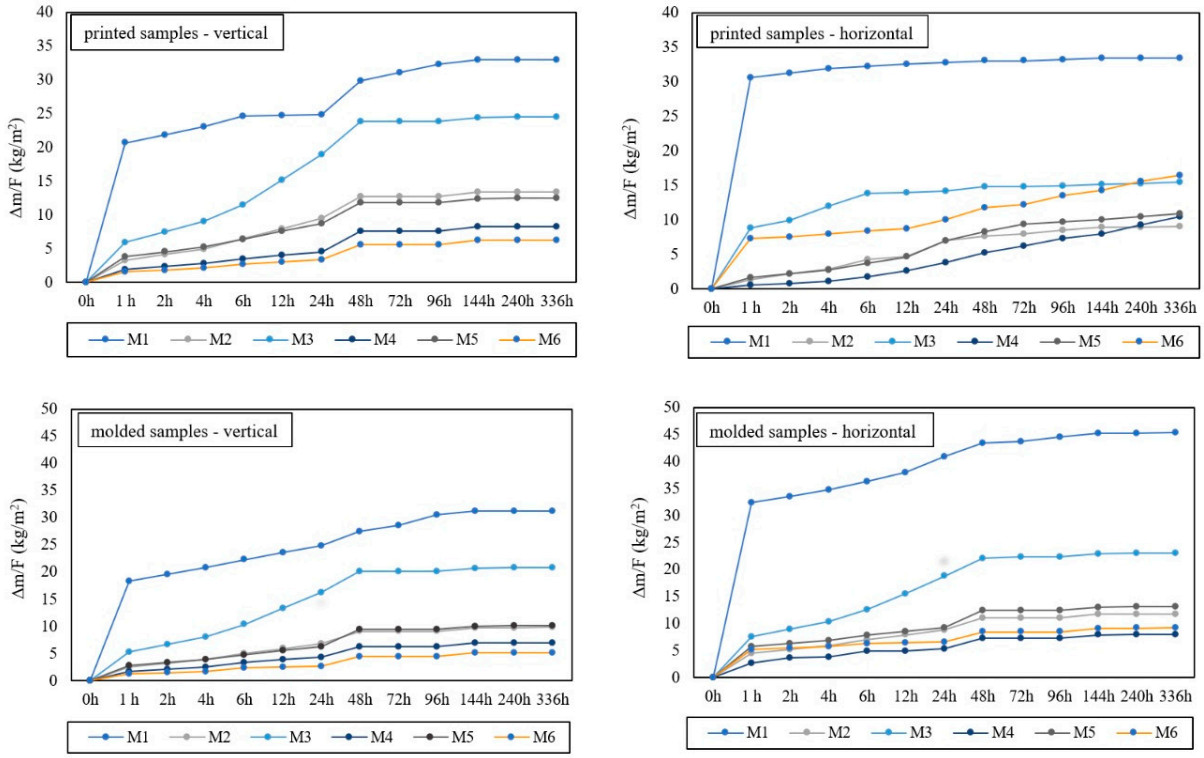


Figure 15. Variations in Δm/F as a function of time, depending on sample orientation, mixture type, and production method.

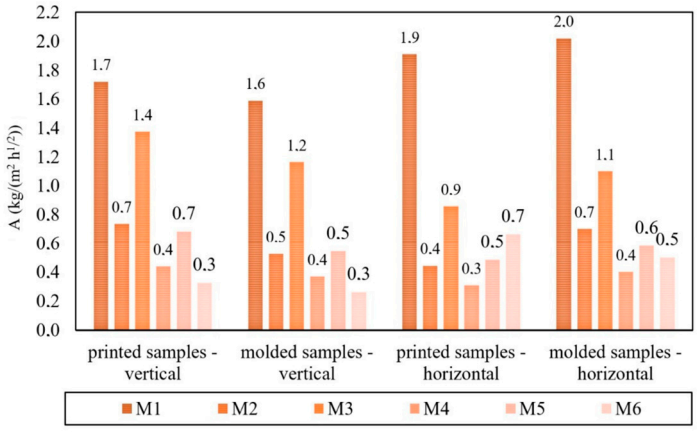
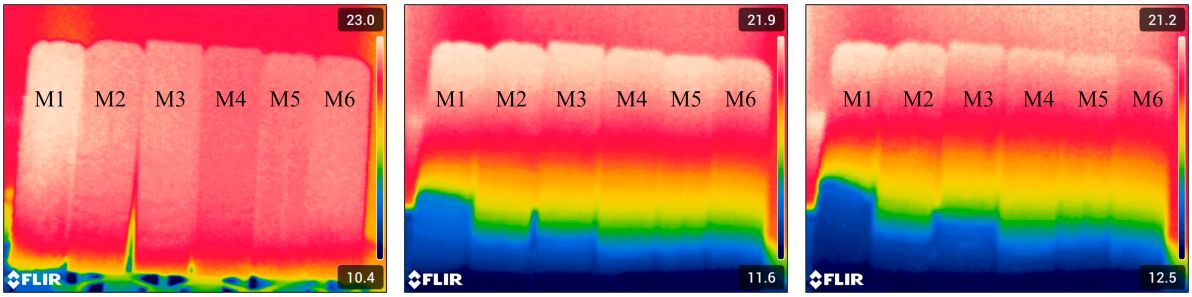


Figure 16. Water sorption coefficient values based on sample orientation, mixture type, and production method.



(**a**) (**b**) (**c**)

Figure 17. Thermal images of samples depending on their composition after water absorption times of: (**a**) 1 min, (**b**) 60 min, and (**c**) 120 min.

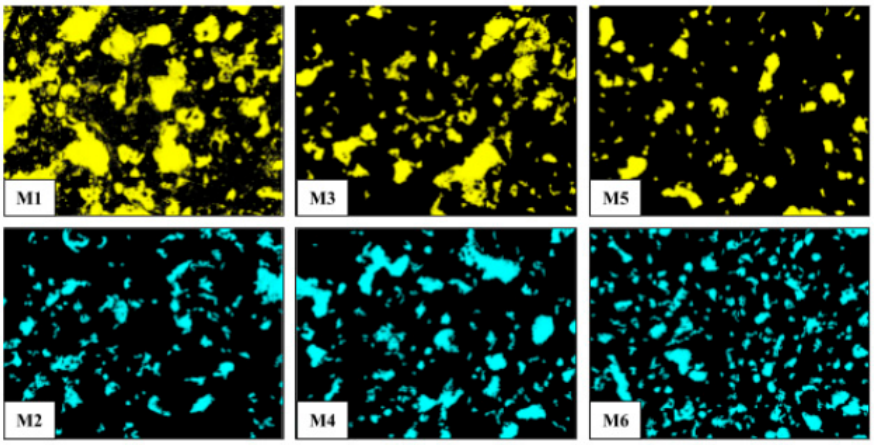


Figure 18. Pores inside 3D printed samples based on mixture type used.

3.5. Microscopy Observation

Microscopic analysis reveals significant differences in the size, shape, and distribution of pores within the material's structure, influenced by the used production methods. As shown in Figure 18, 3D printed samples exhibit greater irregularity in pore shapes. The pores tend to be more oval and flattened, consistent with the theory that the layer-by-layer deposition in printed concrete deforms pores under mechanical pressure and forces during extrusion. As a result, these pores deviate from the ideally spherical shape observed in cast samples. Additionally, the pore sizes in printed samples are more heterogeneous, likely due to variations in printing speeds and the pressure exerted by the nozzle. In contrast, Figure 19 illustrates cast samples with more spherical and uniform pores. This uniformity can be attributed to the natural dispersion of air or foam in the liquid phase during the casting process. The formation of pores in this context is influenced by the minimization of surface energy, leading to shapes closer to a sphere. While minor deformations may occur due to settling and gravity, the overall symmetry of the pores in cast samples remains superior to that observed in printed samples [76–78].

The microscopic images present the porosity of the samples (Figures 18 and 19), revealing large areas that appear completely black, indicating the absence of pores in these regions. These pore-free surfaces are more prominent in the 3D printed samples than in the cast samples. This suggests that the 3D printed specimens have a higher material density, resulting in a less porous structure compared to the cast samples. The layer deposition process in 3D printing, influenced by nozzle pressure, leads to a more compact structure, which causes localized reductions in porosity and an increased number of pore-free areas. In contrast, cast samples exhibit a more homogeneous concrete structure with pores more uniformly distributed, resulting in fewer pore-free areas. Figures 20 and 21 further illustrate

that samples foamed with synthetic agents display larger pores, particularly in the range of 400 to 800 µm. This tendency to form larger pores is likely due to the physical properties of the synthetic agents, which generate larger air bubbles, thereby creating larger pores during the concrete hardening process [79,80]. Figure 20 shows that samples foamed with synthetic agents (AS) exhibit a more varied pore size distribution, with a significant proportion of pores exceeding 400 µm in diameter. In contrast, samples foamed with protein-based agents (PS) display smaller and more uniformly distributed pores. The graphs in Figure 21 reveal that in most cases, pores in the 100–400 µm range dominate, which aligns with findings from previous studies [78]. This distribution indicates that the protein-based foaming agent generates smaller and more homogeneous air bubbles, leading to the formation of smaller, more regular pores throughout the sample. In both AS- and PS-foamed samples, the highest concentration of large pores (400–800 µm) is observed in samples without stabilizers. In contrast, the lowest occurrence of large pores is found in samples stabilized with the commercial stabilizing agent EXOalc 1618, highlighting its effectiveness in reducing the formation of larger voids.

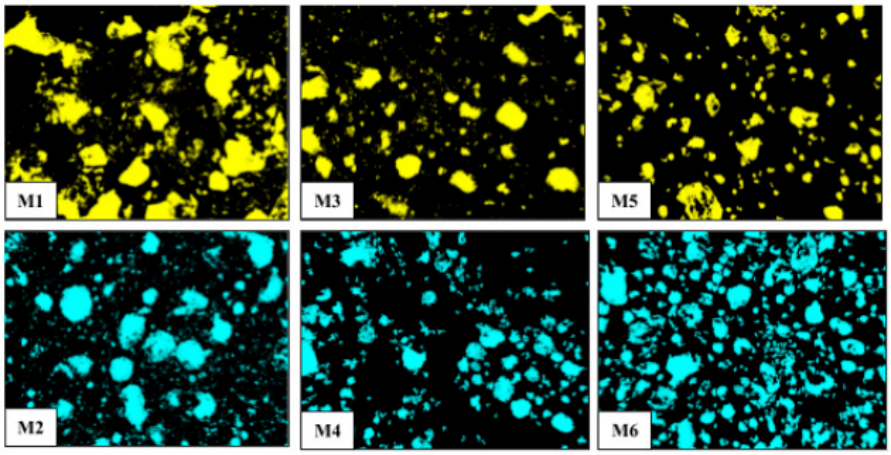


Figure 19. Pores inside molded samples based on mixture type used.

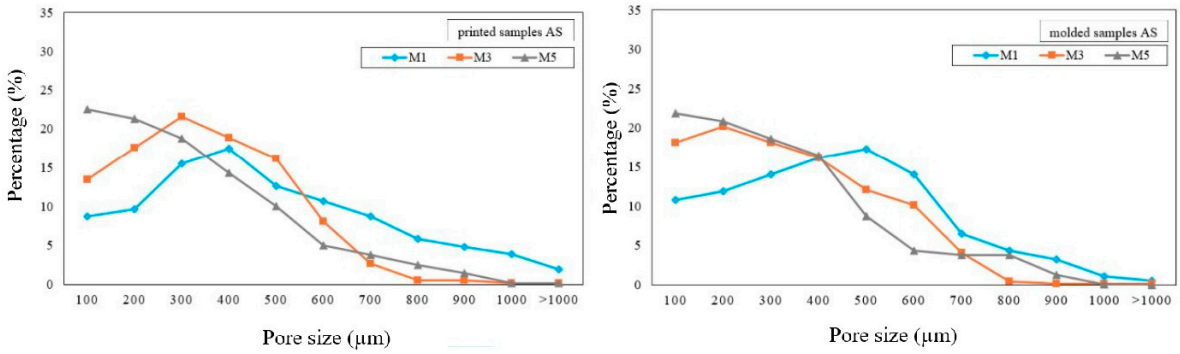


Figure 20. Pore size distribution graph in foamed concrete with synthetic agents based on mixture type used and production method.

Moreover, the stabilizing agents used in samples M3-M6 significantly influence the porosity characteristics of the materials. For samples M3 and M4, which utilized used industrial oil (UO) as a stabilizing agent, greater irregularity in pore shapes and a less uniform distribution of pore sizes were observed. The data indicate that these samples exhibit a higher proportion of pores with varying sizes, suggesting that UO may be less effective in stabilizing the pores, leading to the formation of larger, irregular voids. In contrast, samples M5 and M6, which incorporated the commercial stabilizing agent EXOalc 1618 (CA), demonstrate more uniform and smaller pores, particularly in the 100–400 µm

range. This suggests that the commercial stabilizing agent is more effective in controlling pore formation, resulting in a more stable and predictable concrete structure. The enhanced uniformity in pore size not only contributes to the mechanical properties of the material but also improves its overall performance in various applications.

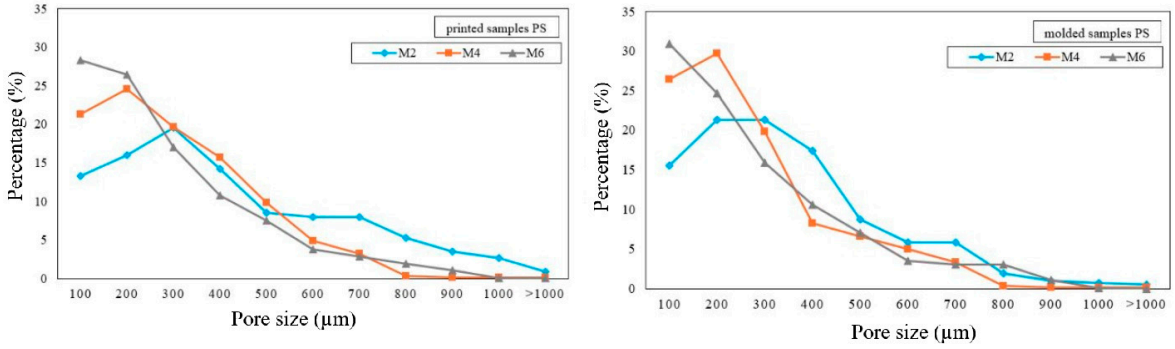


Figure 21. Pore size distribution graph in foamed concrete with protein-based agents based on mixture type used and production method.

Future research will focus on the potential for producing foamed concrete using recycled materials. The priority in these studies will be to develop a stable material with appropriate viscosity and a long open time suitable for 3D printing. An important objective will also be to achieve a material with uniformly distributed pores within the printed sample, which will facilitate the attainment of the desired technological properties required for additive manufacturing processes. Moreover, the use of recycled materials will contribute positively to the sustainable development of the construction industry.

3.6. Flexural Strength Tests and Compressive Strength Tests

A three-point bending test was performed to evaluate the material's behavior under load and its flexural strength. Additionally, two compression tests were conducted, examining the samples in directions parallel and perpendicular to the *Z*-axis, which corresponds to the layer deposition direction in 3D printing. These tests aimed to investigate the influence of load direction on the material's compressive strength and to identify potential anisotropic behavior resulting from the layer-by-layer manufacturing process. The parallel and perpendicular compression tests provided valuable insights into how the printing orientation affects the mechanical performance of the samples.

Figures 22–24 present the results of three-point bending and compression tests conducted as part of this study. The findings indicate that sample M1 exhibits the highest porosity, which correlates with the lowest mechanical strength across all tests. Specifically, the bending strength is limited to 0.2 MPa, and the compressive strength in parallel and perpendicular directions is 0.2 MPa and 0.1 MPa, respectively. The elevated porosity significantly compromises the material's structural integrity, hindering effective load transfer. In contrast, samples foamed with synthetic agents with stabilizer additions M3 and M5 display reduced and more uniform porosity compared to M1. For sample M3, the bending strength is 1 MPa, while the compressive strengths in the parallel and perpendicular directions are 8.1 MPa and 4.2 MPa, respectively. The favorable compression results suggest a more optimal pore distribution within this sample. Sample M5, meanwhile, achieves a bending strength of 1.7 MPa, a parallel compressive strength of approximately 4.3 MPa, and an impressive strength of 11.5 MPa in the perpendicular direction. These results suggest that the presence of fewer pores with more regular shapes and smaller surface areas contributes to the enhancement of the mechanical properties.



Figure 22. Flexural test depending on the sample composition.



Figure 23. Compressive strength of samples in the direction parallel to the *Z*-axis (layer deposition direction) depending on the sample composition.



Figure 24. Compressive strength of samples in the direction perpendicular to the *Z*-axis (layer deposition direction) depending on the sample composition.

The PS-foamed samples, namely M2, M4, and M6, are characterized by significantly more regular porosity. These samples exhibit the highest strength values. M4 and M6 demonstrate bending strengths of 1.4 MPa and 3.8 MPa, respectively, along with the highest compressive strengths in the perpendicular direction (7.8 MPa and 10.3 MPa) and parallel direction (10 MPa and 4.3 MPa). These findings suggest that the uniform distribution of pores, despite their high quantity, enables effective load transfer and minimizes stress concentration. Sample M2, however, yields more moderate results, with 1.6 MPa in bending, 6.2 MPa in parallel compression, and 3.5 MPa in perpendicular compression. These values suggest a relatively limited influence of pores on the material's strength compared to the other samples. The results clearly differentiate between CA-stabilized samples regardless of the foaming agent used. Samples subjected to compression perpendicular to the layer

deposition direction exhibit the highest strength values (M5: 11.5 MPa and M6: 10.3 MPa), while those tested parallel to the deposition direction display strength values nearly three times lower. This discrepancy may be attributed to the 3D printing process, in which the layers of rapidly emulsified material may not bond sufficiently, leading to a reduction in mechanical strength along the direction parallel to the print. The weaker connections between individual layers likely result in diminished load transfer in this direction, as evidenced by Figure 11, where the upper layers of the prints appear narrower due to the denser material flow from the extruder.

4. Conclusions

Research on foam concrete, considering the influence of foaming agents and stabilizers on porosity and structural stability, mechanical properties, and thermal insulation, is essential for the development of 3D concrete printing technology, as well as sustainable construction practices. A strong dependence was identified between apparent density and water absorption properties. A synthetic foaming agent (AS) allows for a lower material density than a protein-based foaming agent, which is advantageous for lightweight construction materials. On the other hand, the stabilizer CA significantly enhances concrete foam stability, albeit at the cost of increased density. Without a stabilizer, AS foam exhibited significant degradation within 30 min, with noticeable bubble reduction by 15 min. The UO stabilizer improved stability markedly, with bubbles persisting longer despite coalescence. The CA stabilizer also enhanced stability, but the difference was not significant compare to UO, showing moderate degradation within the 30 min observation period. PS foam without a stabilizer degraded during the experiment. The UO stabilizer significantly increased foam durability, with minimal degradation during the observation period. The CA stabilizer provided stabilization, maintaining an almost unchanged bubble structure during 30 min. Mixtures prepared with the synthetic foaming agent in the absence of stabilizers (M1) exhibited the highest water absorption rates. In contrast, the addition of stabilizers, particularly formulations incorporating cetearyl and stearyl alcohol (M5 and M6), markedly reduced water absorption. Samples with the addition of the synthetic foaming agent (M1, M3, M5) generally showed higher water sorption coefficients compared to those with the protein-based foaming agent (M2, M4, M6). The highest sorption values were observed in samples M1 (1.7 $kg/m^2h^{1/2}$) and M3 (1.6 $kg/m^2h^{1/2}$) in the vertical orientation, with the horizontal orientation of sample M3 achieving a peak value of 2.0 $kg/m^2h^{1/2}$. Moreover, stabilization using UO (M3, M4) resulted in higher sorption coefficients than stabilization with CA (M5, M6). A microscopic analysis of porosity revealed notable differences between 3D printed and cast samples. The 3D printed specimens exhibited higher material density and a more compact structure, characterized by reduced porosity and increased pore-free regions. This densification is attributed to the layer-by-layer deposition process and nozzle pressure, which contribute to a tighter packing of the material. Furthermore, the choice of foaming agent significantly influenced pore morphology: synthetic foaming agents produced larger, irregularly shaped pores, while protein-based agents caused smaller, more uniform pores. The stabilizing agents also determined porosity characteristics. Stabilization with UO resulted in greater irregularity in pore distribution, whereas commercial stabilizers like CA generated smaller, more uniformly distributed pores. Sample M1, with the highest porosity, exhibited the weakest mechanical properties, including a bending strength of 0.2 MPa, parallel compressive strength of 0.2 MPa, and perpendicular compressive strength of 0.1 MPa. In contrast, samples with reduced and more uniform porosity, such as M5 and M6, achieved higher strength values, with M5 displaying a perpendicular compressive strength of 11.5 MPa and bending strength of 1.7 MPa. Synthetic foaming agents with stabilizers (e.g., M3, M5) and PS-foamed samples (M4, M6) exhibited enhanced mechani-

cal performance. M6 achieved the highest bending strength (3.8 MPa) and compressive strengths of 4.3 MPa (parallel) and 10.3 MPa (perpendicular), attributed to uniform pore distribution minimizing stress concentration. Compression strength perpendicular to the layer deposition direction (M5: 11.5 MPa; M6: 10.3 MPa) was significantly higher than in the parallel direction, where strength values were up to three times lower. This disparity is linked to weaker interlayer bonding in the 3D printing process, highlighting a need to optimize layer adhesion to improve load transfer. The improved pore uniformity in CA-stabilized samples corresponded to enhanced mechanical properties and overall performance, emphasizing the critical role of both foaming and stabilizing agents in optimizing the porosity and structural integrity of foam concrete. The utilization of finely ground brick particles as a foam stabilizer in concrete presents a promising alternative for improving material performance. Future research should focus on investigating the effects of varying GB proportions on foam stability and overall concrete properties. Similarly to fine particles like nano-silica, nano-calcium carbonate, or nano-alumina, GB has the potential to enhance foam stability, improve the mechanical properties of foam concrete, and contribute to sustainable construction by addressing waste management challenges.

Author Contributions: Conceptualization, M.R. and M.H.; Methodology, M.R., M.M., A.H., M.G., K.R.-Ż. and M.H.; Software: M.R, M.M., A.H. and M.H.; Validation, M.H.; Formal analysis, M.R. and M.H.; Investigation, M.R., M.M., A.H. and K.R.-Ż.; Resources, M.H.; Data curation, M.M., A.H., M.G. and K.R.-Ż.; Writing—original draft, M.R. and M.H.; Writing—review & editing, M.R. and M.H.; Visualization, M.R.; Supervision, M.H.; Project administration, M.H.; Funding acquisition, M.H. All authors have read and agreed to the published version of the manuscript.

Funding: This research has been supported by the Ministry of Science and Higher Education within the program "Implementation Doctorate".

Data Availability Statement: The original contributions presented in this study are included in the article. Further inquiries can be directed to the corresponding author.

Conflicts of Interest: The authors declare no conflicts of interest.

References

1. Adhikary, S.; Rudžionis, Z.; Tučkutė, S. Characterization of novel lightweight self-compacting cement composites with incorporated expanded glass, aerogel, zeolite and fly ash. *Case Stud. Constr. Mater.* **2022**, *16*, e00879. [CrossRef]
2. Chen, G.; Li, F.; Jing, P.; Geng, J.; Si, Z. Effect of Pore Structure on Thermal Conductivity and Mechanical Properties of Autoclaved Aerated Concrete. *Materials* **2021**, *14*, 339. [CrossRef]
3. He, L.; Xinpeng, Z. Thermal Conductivity Analysis of High Porosity Structures with Open and Closed Pores. *Int. J. Heat Mass Transf.* **2022**, *183 Pt A*, 122089. [CrossRef]
4. Chen, G.; Li, F.; Geng, J.; Jing, P.; Si, Z. Identification, generation of autoclaved aerated concrete pore structure and simulation of its influence on thermal conductivity. *Constr. Build. Mater.* **2021**, *294*, 123572. [CrossRef]
5. Xu, Y.; Tong, S.; Xu, X.; Mao, J.; Kang, X.; Luo, J.; Jiang, L.; Guo, M.Z. Effect of foam stabilization on the properties of foamed concrete modified by expanded polystyrene. *J. Build. Eng.* **2023**, *73*, 106822. [CrossRef]
6. Cho, S.; Rooyen, V.; Kearsley, E.; Zijl, G. Foam stability of 3D printable foamed concrete. *J. Build. Eng.* **2022**, *47*, 103884. [CrossRef]
7. Wang, J.; Nguyen, A.; Farrokhpay, S. A Critical Review of the Growth, Drainage and Collapse of Foams. *Adv. Colloid Interface Sci.* **2016**, *228*, 55–70. [CrossRef]
8. Feneuil, B.; Roussel, N.; Pitois, O. Optimal cement paste yield stress for the production of stable cement foams. *Cem. Concr. Res.* **2019**, *120*, 142–151. [CrossRef]
9. Feneuil, B. Cement Foam Stability: Link with Cement Paste Rheological Properties. Doctoral Dissertation, Université Paris-Est, Paris, France, 2018. Available online: https://pastel.hal.science/tel-02084040/file/TH2018PESC1045.pdf (accessed on 7 January 2025).
10. Feneuil, B.; Aimedieu, P.; Scheel, M.; Perrin, J.; Roussel, N.; Pitois, O. Stability criterion for fresh cement foams. *Cem. Concr. Res.* **2019**, *125*, 105865. [CrossRef]
11. Yanagisawa, N.; Kurita, R. In-situ observation of collective bubble collapse dynamics in a quasi-two-dimensional foam. *Sci. Rep.* **2019**, *9*, 5152. [CrossRef] [PubMed]

12. Falliano, D.; Restuccia, L.; Gugliandolo, E. A simple optimized foam generator and a study on peculiar aspects concerning foams and foamed concrete. *Constr. Build. Mater.* **2020**, *268*, 121101. [CrossRef]
13. Jiang, L.; Wang, Z.; Gao, X.; Cui, M.; Yang, Q.; Qin, J. Effect of nanoparticles and surfactants on properties and microstructures of foam and foamed concrete. *Constr. Build. Mater.* **2024**, *411*, 134444. [CrossRef]
14. Chen, Y. Experimental study on application performance of foamed concrete prepared based on a colloidal NanoSiO_2-stabilized foam. *Constr. Build. Mater.* **2023**, *409*, 134012. [CrossRef]
15. Xiong, Y.; Zhu, Y.; Chen, C.; Zhang, Y. Effect of nano-alumina modified foaming agents on properties of foamed concrete. *Constr. Build. Mater.* **2023**, *267*, 121045. [CrossRef]
16. Zhang, H.; Wang, Z.; Zhang, T.; Li, Z. Foam Stabilization Process for Nano-Al2O3 and Its Effect on Mechanical Properties of Foamed Concrete. *Nanomaterials* **2024**, *14*, 1516. [CrossRef]
17. Song, N.; Li, Z.; Yi, W.; Wang, S. Properties of foam concrete with hydrophobic starch nanoparticles as foam stabilizer. *J. Build. Eng.* **2022**, *56*, 104811. [CrossRef]
18. Song, N.; Li, Z.; Wang, S.; Li, G. Preparation of biomass carbon dots for foam stabilizer of foamed concrete. *Constr. Build. Mater.* **2023**, *364*, 129853. [CrossRef]
19. Chen, H.; Liang, K.; Chow, C.L.; Lau, D. Enhancing the engineering performance of lightweight limestone calcined clay cement concrete using used engine oil as a foam stabilizer. *J. Build. Eng.* **2024**, *95*, 110187. [CrossRef]
20. Qi, X.; Bao, Y.; Wang, W.; Zhang, S.; Wu, Y.; Jia, Z.; Guo, S. Superior performance foamed concrete fabricated with amphiphilic and hydrophilic particles stabilized ultra-stable foam. *Cem. Concr. Compos.* **2024**, *152*, 105613. [CrossRef]
21. Vincent, P.; Eswari, R.P.; Theenathayalan, R.; Suganya, R. Prediction of foam stability for synthetic anionic ammonium-based surfactants having identical hydrophilic head group. *Asian J. Civ. Eng.* **2023**, *24*, 2481–2490. [CrossRef]
22. Hamza, A.; Kocserha, I. The Investigation of Sodium Lauryl Sulphate as Foam Stabilizer in Cement Foams. *Mater. Sci. Eng.* **2020**, *45*, 115–124.
23. Moutaoukil, G.; Sobrados, I.; Alehyen, S.A.; Taibi, M. Understanding the thermomechanical behavior of geopolymer foams: Influence of rate and type of foaming agent and stabilizer. *Chem. Data Collect.* **2024**, *50*, 101111. [CrossRef]
24. Maglad, A.M.; Mydin, M.A.O.; Datta, S.D.; Abbood, I.S.; Tayeh, B.A. Impact of anionic surfactant-based foaming agents on the properties of lightweight foamed concrete. *Constr. Build. Mater.* **2024**, *438*, 137119. [CrossRef]
25. Abdollahnejad, Z.; Pacheco-Torgal, F.; Félix, T.; Tahri, W.; Aguiar, J.B. Mix design, properties and cost analysis of fly ash-based geopolymer foam. *Constr. Build. Mater.* **2015**, *80*, 18–30. [CrossRef]
26. Zhu, H.; Chen, L.; Xu, J.; Han, Q. Experimental study on performance improvement of anionic surfactant foaming agent by xanthan gum. *Constr. Build. Mater.* **2020**, *230*, 116993. [CrossRef]
27. Wei, X.; Wang, H.; Xie, Y.; Du, Y. An experimental investigation on the effect of carboxymethyl cellulose on morphological characteristics of dust-suppression foam and its mechanism exploration. *Process. Saf. Environ. Prot.* **2020**, *135*, 126–134. [CrossRef]
28. Gu, X.; Wang, S.; Liu, J.; Wang, H.; Xu, X.; Wang, Q.; Zhu, Z. Effect of hydroxypropyl methyl cellulose (HPMC) as foam stabilizer on the workability and pore structure of iron tailings sand autoclaved aerated concrete. *Constr. Build. Mater.* **2023**, *376*, 130979. [CrossRef]
29. Liu, C.; Wang, X.; Chen, Y.; Zhang, C.; Ma, L.; Deng, Z.; Chen, C.; Zhang, Y.; Pan, J.; Banthia, N. Influence of hydroxypropyl methylcellulose and silica fume on stability, rheological properties, and printability of 3D printing foam concrete. *Cem. Concr. Compos.* **2021**, *122*, 104158. [CrossRef]
30. Cui, J.; He, Z.; Zhang, G.; Cai, X. Rheological properties of sprayable ultra-high performance concrete with different viscosity-enhancing agents. *Constr. Build. Mater.* **2022**, *321*, 126154. [CrossRef]
31. Liu, C.; Chen, Y.; Xiong, Y.; Jia, L.; Ma, L.; Wang, X.; Chen, C.; Banthia, N.; Zhang, Y. Influence of HPMC and SF on buildability of 3D printing foam concrete: From water state and flocculation point of view. *Compos. Part B Eng.* **2022**, *242*, 110075. [CrossRef]
32. She, W.; Du, Y.; Miao, C.; Liu, J.; Zhao, G.; Jiang, J.; Zhang, Y. Application of organic-and nanoparticle-modified foams in foamed concrete: Reinforcement and stabilization mechanisms. *Cem. Concr. Res.* **2018**, *106*, 12–22. [CrossRef]
33. Othman, R.; Jaya, R.P.; Muthusamy, K.; Sulaiman, M.; Duraisamy, Y.; Abdullah, M.M.A.B.; Przybył, A.; Sochacki, W.; Skrzypczak, T.; Vizureanu, P.; et al. Relation between Density and Compressive Strength of Foamed Concrete. *Materials* **2021**, *14*, 2967. [CrossRef] [PubMed]
34. Pasupathy, K.; Ramakrishnan, S.; Sanjayan, J. Enhancing the properties of foam concrete 3D printing using porous aggregates. *Cem. Concr. Compos.* **2022**, *133*, 104687. [CrossRef]
35. Al-Ani, H.K.K.; Hilal, A.A.; Hama, S.M. Effect of Finesse and Type of Aggregate on Flowability and Mechanical Properties of Foamed Concrete. *E3S Web Conf.* **2023**, *427*, 02009. [CrossRef]
36. Amran, M.; Fediuk, R.; Vatin, N.; Murali, G.; Ozbakkaloglu, T.; Klyuev, S.; Alabduljabber, H. Fibre-Reinforced Foamed Concretes: A Review. *Materials* **2020**, *13*, 4323. [CrossRef]
37. Bian, P.; Zhang, M.; Yu, Q.; Zhan, B.; Gao, P.; Guo, B.; Chen, Y. Prediction model of compressive strength of foamed concrete considering pore size distribution. *Constr. Build. Mater.* **2023**, *409*, 133705. [CrossRef]

38. Gökçe, H.S.; Hatungimana, D.; Ramyar, K. Effect of fly ash and silica fume on hardened properties of foam concrete. *Constr. Build. Mater.* **2019**, *194*, 1–11. [CrossRef]
39. Diagne, M.; Dia, I.; Gueye, O. Influence of Types of Fillers on Workability, Bleeding, Compressive Strength, and Degree of Compaction of Hydraulic Concrete. *Mater. Sci. Appl.* **2021**, *12*, 276–296. [CrossRef]
40. Hou, L.; Li, J.; Lu, Z.; Niu, Y. Influence of foaming agent on cement and foam concrete. *Constr. Build. Mater.* **2021**, *280*, 122399. [CrossRef]
41. Zhang, N.; Sanjayan, J. Quick nozzle mixing technology for 3D printing foam concrete. *J. Build. Eng.* **2024**, *83*, 108445. [CrossRef]
42. Rudziewicz, M.; Maroszek, M.; Setlak, K.; Góra, M.; Hebda, M. Optimization of Foams-Polypropylene Fiber-Reinforced Concrete Mixtures Dedicated for 3D Printing. *Materials* **2024**, *17*, 4106. [CrossRef]
43. Mohamed, A.M.; Tayeh, B.A.; Majeed, S.S.; Aisheh, Y.I.A.; Salih, M.N.A. Ultra-light foamed concrete mechanical properties and thermal insulation perspective: A comprehensive review. *J. CO_2 Util.* **2024**, *83*, 102827. [CrossRef]
44. Markin, V.; Nerella, V.N.; Schröfl, C.; Guseynova, G.; Mechtcherine, V. Material Design and Performance Evaluation of Foam Concrete for Digital Fabrication. *Materials* **2019**, *12*, 2433. [CrossRef] [PubMed]
45. Markin, V.; Krause, M.; Otto, J.; Schröfl, C.; Mechtcherine, V. 3D-printing with foam concrete: From material design and testing to application and sustainability. *J. Build. Eng.* **2021**, *43*, 102870. [CrossRef]
46. Rehman, A.U.; Kim, J.-H. 3D Concrete Printing: A Systematic Review of Rheology, Mix Designs, Mechanical, Microstructural, and Durability Characteristics. *Materials* **2021**, *14*, 3800. [CrossRef]
47. Zhang, C.; Nerella, V.N.; Krishna, A.; Wang, S.; Zhang, Y.; Mechtcherine, V.; Banthia, N. Mix design concepts for 3D printable concrete: A review. *Cem. Concr. Compos.* **2021**, *122*, 104155. [CrossRef]
48. Available online: https://budowlana-chemia.com/pl/p/PIANOBETON-Pianotwor-10-L./318 (accessed on 7 January 2025).
49. Available online: https://www.products.pcc.eu/wp-content/uploads/import/product/broszura/d43bec7c-1e79-46c8-9ea3-3074fb73799d/exoalc-1618-pastylki_broszura_en.pdf (accessed on 7 January 2025).
50. Hajer, A.; Ali, S.; Hameed, A.H. Using recycled bricks to improve the compressive strength of concrete and produce lightweight concrete. *Herit. Sustain. Dev.* **2023**, *5*, 175–182. [CrossRef]
51. Chen, D.; Chen, M.; Zhou, X.; Wu, Y.; Jiang, Q.; Yang, X.; Zhao, Y.; Zhang, J. Effects of waste cooking oil derivatives as a foam stabilizer on properties of foam and foamed geopolymer concrete. *Constr. Build. Mater.* **2024**, *450*, 138675. [CrossRef]
52. Kashani, A.; Ngo, T.; Tuan; Nguyen, T.; Hajimohammadi, A.; Sinaie, S.; Mendis, P. The effects of surfactants on properties of lightweight concrete foam. *Mag. Concr. Res.* **2018**, *72*, 163–172. [CrossRef]
53. Testing Fresh Concrete—Part 5: Flow Table Test PN-EN 12350-5:2019-08. Available online: https://wiedza.pkn.pl/wyszukiwarka-norm?ref=PN-EN%2012350-5:2019-08E (accessed on 30 July 2024).
54. *PN-EN ISO 178*; Plastics—Determination of Flexural Properties. PKN: Warsaw, Poland, 2011.
55. *EN 12390-3*; Testing Hardened Concrete—Part 3: Compressive Strength of Test Specimens. CEN: Brussels, Belgium, 2009.
56. Dhasindrakrishna, K.; Ramakrishnan, S.; Pasupathy, K.; Sanjayan, J. Collapse of fresh foam concrete: Mechanisms and influencing parameters. *Cem. Concr. Compos.* **2021**, *122*, 104151. [CrossRef]
57. Dhasindrakrishna, K.; Pasupathy, K.; Ramakrishnan, S.; Sanjayan, J. Effect of yield stress development on the foam-stability of aerated geopolymer concrete. *Cem. Concr. Res.* **2020**, *138*, 106233. [CrossRef]
58. Du, X.; Zhao, L.; He, X.; Chen, H.; Fang, W.; Li, W. Ultra-stable aqueous foams with multilayer films stabilized by 1-dodecanol, sodium dodecyl sulfonate and polyvinyl alcohol. *Chem. Eng. Sci.* **2017**, *160*, 72–79. [CrossRef]
59. Zeng, X.; Lan, X.; Zhu, H.; Liu, H.; Umar, H.A.; Xie, Y.; Long, G.; Ma, C. A Review on Bubble Stability in Fresh Concrete: Mechanisms and Main Factors. *Materials* **2020**, *12*, 1820. [CrossRef] [PubMed]
60. Samad, N.; Abdullah, S.; Ibrahim, M.; Shahidan, S.; Ismail, N. Initial properties of 3D printing concrete using Rice Husk Ash (RHA) as Partial Cement Replacement. *IOP Conf. Ser. Earth Environ. Sci.* **2022**, *1022*, 012055. [CrossRef]
61. Nodehi, M.; Ozbakkaloglu, T.; Gholampour, A. Effect of supplementary cementitious materials on properties of 3D printed conventional and alkali-activated concrete: A review. *Autom. Constr.* **2022**, *138*, 104215. [CrossRef]
62. Wang, X.; Li, W.; Guo, Y.; Kashani, A.; Wang, K.; Ferrara, L.; Agudelo, I. Concrete 3D printing technology for sustainable construction: A review on raw material, concrete type and performance. *Dev. Built Environ.* **2024**, *17*, 100378. [CrossRef]
63. Lee, J.; Kim, J. Matric suction of fine sand and its effect on the shape stability of 3D printed cement mortar. *Constr. Build. Mater.* **2022**, *341*, 127618. [CrossRef]
64. da Silveira Júnior, J.G.; de Moura Cerqueira, K.; de Araújo Moura, R.C.; de Matos, P.R.; Rodriguez, E.D.; de Castro Pessôa, J.R.; Souza, M.T. Influence of Time Gap on the Buildability of Cement Mixtures Designed for 3D Printing. *Buildings* **2024**, *14*, 1070. [CrossRef]
65. Tu, H.; Wei, Z.; Bahrami, A.; Kahla, N.B.; Ahmad, A.; Özkılıç, Y.O. Recent advancements and future trends in 3D concrete printing using waste materials. *Dev. Built Environ.* **2023**, *16*, 100187. [CrossRef]
66. Hager, I.; Maroszek, M.; Mróz, K.; Kęsek, R.; Hebda, M.; Dvorkin, L.; Marchuk, V. Interlayer Bond Strength Testing in 3D-Printed Mineral Materials for Construction Applications. *Materials.* **2022**, *15*, 4112. [CrossRef] [PubMed]

67. Hashim, M.; Tantray, M. Comparative study on the performance of protein and synthetic-based foaming agents used in foamed concrete. *Case Stud. Constr. Mater.* **2021**, *14*, e00524. [CrossRef]
68. Gołaszewski, J.; Klemczak, B.; Smolana, A.; Gołaszewska, M.; Cygan, G.; Mankel, C.; Peralta, I.; Röser, F.; Koenders, E.A.B. Effect of Foaming Agent, Binder and Density on the Compressive Strength and Thermal Conductivity of Ultra-Light Foam Concrete. *Buildings* **2022**, *12*, 1176. [CrossRef]
69. Rahul, A.V.; Santhanam, M.; Meena, H.; Ghani, Z. Mechanical characterization of 3D printable concrete. *Constr. Build. Mater.* **2019**, *227*, 116710. [CrossRef]
70. Abdullah, I.M.; Adisalamun; Rinaldi, W. Foam Agent Synthesis for the Production of Foam-Based Concrete. *J. Appl. Technol.* **2023**, *10*, 17–23.
71. Xiong, Y.; Baoliang, L.; Chun, C.; Yamei, Z. Properties of foamed concrete with Ca(OH)2 as foam stabilizer. *Cem. Concr. Compos.* **2021**, *118*, 103985. [CrossRef]
72. Ji, Y.; Sun, Q. The Stabilizing Effect of Carboxymethyl Cellulose on Foamed Concrete. *Int. J. Mol. Sci.* **2022**, *7*, 15473. [CrossRef]
73. Liu, X.; Li, S.; Duan, Y.; Du, Z.; Zuo, X.; Dong, J.; Cheng, H. Influence of Printing Interval on the Imbibition Behavior of 3D-Printed Foam Concrete for Sustainable and Green Building Applications. *Sustainability* **2024**, *16*, 7841. [CrossRef]
74. Fan, G.; Xiang, W.; Yang, J.; Yang, S.; Xiang, C. Study on Capillary Water Absorption of Waterborne-Polyurethane-Modified Recycled Coarse Aggregate Concrete. *Polymers* **2023**, *15*, 3860. [CrossRef] [PubMed] [PubMed Central]
75. Shawnim, P.; Mohammad, F. Porosity, Permeability and Microstructure of Foamed Concrete through SEM Images. *J. Civ. Eng. Sci. Technol.* **2019**, *10*, 22–33. [CrossRef]
76. Pasupathy, K.; Ramakrishnan, S.; Sanjayan, J. Fresh and Hardened Properties of 3D Printable Foam Concrete Containing Porous Aggregates. In Proceedings of the Third RILEM International Conference on Concrete and Digital Fabrication, Loughborough, UK, 27–29 June 2022; Volume 37. [CrossRef]
77. Jiang, S.; Wang, Y.; Hua, S.; Yue, H.; Zhang, Y. Preparation and Performance Characterization of Low-Density 3D-Printed Expanded Perlite–Foam Concrete. *Appl. Sci.* **2024**, *14*, 6796. [CrossRef]
78. Gencel, O.; Bilir, T.; Bademler, Z.; Ozbakkaloglu, T. A Detailed Review on Foam Concrete Composites: Ingredients, Properties, and Microstructure. *Appl. Sci.* **2022**, *12*, 5752. [CrossRef]
79. Rudziewicz, M.; Maroszek, M.; Góra, M.; Dziura, P.; Mróz, K.; Hager, I.; Hebda, M. Feasibility Review of Aerated Materials Application in 3D Concrete Printing. *Materials.* **2023**, *16*, 6032. [CrossRef]
80. Pasupathy, K.; Ramakrishnan, S.; Sanjayan, J. Influence of recycled concrete aggregate on the foam stability of aerated geopolymer concrete. *Constr. Build. Mater.* **2021**, *271*, 121850. [CrossRef]

Disclaimer/Publisher's Note: The statements, opinions and data contained in all publications are solely those of the individual author(s) and contributor(s) and not of MDPI and/or the editor(s). MDPI and/or the editor(s) disclaim responsibility for any injury to people or property resulting from any ideas, methods, instructions or products referred to in the content.